Stem Cell Reports
Report
OPEN ACCESS

CRIPTO/GRP78 Signaling Maintains Fetal and Adult Mammary Stem Cells Ex Vivo

Benjamin T. Spike,[1,*] Jonathan A. Kelber,[3,4] Evan Booker,[2] Madhuri Kalathur,[2] Rose Rodewald,[1] Julia Lipianskaya,[1] Justin La,[1] Marielle He,[2] Tracy Wright,[3] Richard Klemke,[3] Geoffrey M. Wahl,[1] and Peter C. Gray[2,*]

[1]Gene Expression Laboratory, The Salk Institute for Biological Studies, La Jolla, CA 92037, USA
[2]Clayton Foundation Laboratories for Peptide Biology, The Salk Institute for Biological Studies, La Jolla, CA 92037, USA
[3]Department of Pathology, University of California, San Diego, La Jolla, CA 92037, USA
[4]Present address: Department of Biology, California State University, Northridge, CA 91330, USA
*Correspondence: bspike@salk.edu (B.T.S.), gray@salk.edu (P.C.G.)
http://dx.doi.org/10.1016/j.stemcr.2014.02.010

SUMMARY

Little is known about the extracellular signaling factors that govern mammary stem cell behavior. Here, we identify CRIPTO and its cell-surface receptor GRP78 as regulators of stem cell behavior in isolated fetal and adult mammary epithelial cells. We develop a CRIPTO antagonist that promotes differentiation and reduces self-renewal of mammary stem cell-enriched populations cultured ex vivo. By contrast, CRIPTO treatment maintains the stem cell phenotype in these cultures and yields colonies with enhanced mammary gland reconstitution capacity. Surface expression of GRP78 marks CRIPTO-responsive, stem cell-enriched fetal and adult mammary epithelial cells, and deletion of GRP78 from adult mammary epithelial cells blocks their mammary gland reconstitution potential. Together, these findings identify the CRIPTO/GRP78 pathway as a developmentally conserved regulator of fetal and adult mammary stem cell behavior ex vivo, with implications for the stem-like cells found in many cancers.

INTRODUCTION

Somatic stem cells govern the development, maintenance, and regeneration of tissues, and their dysregulation is associated with diverse pathologies, including cancer. Given the significance of these cells both biologically and therapeutically, it is critical to define factors and signaling mechanisms that dictate their behavior, including those that define niches capable of promoting the stem cell phenotype in normal and disease settings. However, few such factors have been elucidated, and progress toward this goal has been impeded by the fact that most somatic stem cells, including those of the mammary gland, are rare and difficult to isolate and propagate ex vivo.

The mammary epithelium consists principally of lineage-restricted basal keratin-14-positive ($KRT14^+$) myoepithelial cells and keratin-8-positive ($KRT8^+$) luminal epithelial cells (Mikaelian et al., 2006). Although recent reports indicate extensive self-renewal within each of these lineage-committed populations (Van Keymeulen et al., 2011), classic single-cell transplant experiments indicate the presence of rare transplantable bipotent mammary stem cells (MaSCs) in the mature mammary gland (Shackleton et al., 2006). These cells can be significantly enriched through the use of cell-surface marker combinations such as CD24 and CD49f (Stingl et al., 2006). However, the functional significance of such markers to stem cell biology is often unclear, and the resulting enrichment generally remains too low to discern core molecular determinants of the stem cell state from the population at large.

In an effort to circumvent these challenges, we recently characterized a highly enriched population of stem cells from murine embryonic mammary rudiments (Spike et al., 2012). The greater purity of these fetal mammary stem cells (fMaSC) relative to their adult counterparts makes them particularly useful in the study of MaSC biology. Interestingly, we found that fMaSCs share gene expression features with certain aggressive human breast cancers that are not shared between enriched populations of adult MaSCs and the same breast cancers. This distinction may reflect intrinsic differences between the fetal and adult MaSCs or differential heterogeneity in the stem cell-enriched populations used for profiling. Alternatively, this observation may be due to critical differences in the tissue contexts from which these cells are derived, a possibility consistent with prior reports indicating an important role for microenvironmental factors in establishing and maintaining the stem cell competence of both fetal and adult mammary cells (Makarem et al., 2013; Spike et al., 2012; Vaillant et al., 2011). However, the ability of specific factors to promote the MaSC phenotype has rarely been directly demonstrated.

CRIPTO (CR-1, *TDGF1*) is an oncofetal, GPI-anchored/secreted signaling protein that plays key roles as a stem cell regulator (Adewumi et al., 2007; Bianco et al., 2010; Hough et al., 2009; Miharada et al., 2011). CRIPTO is

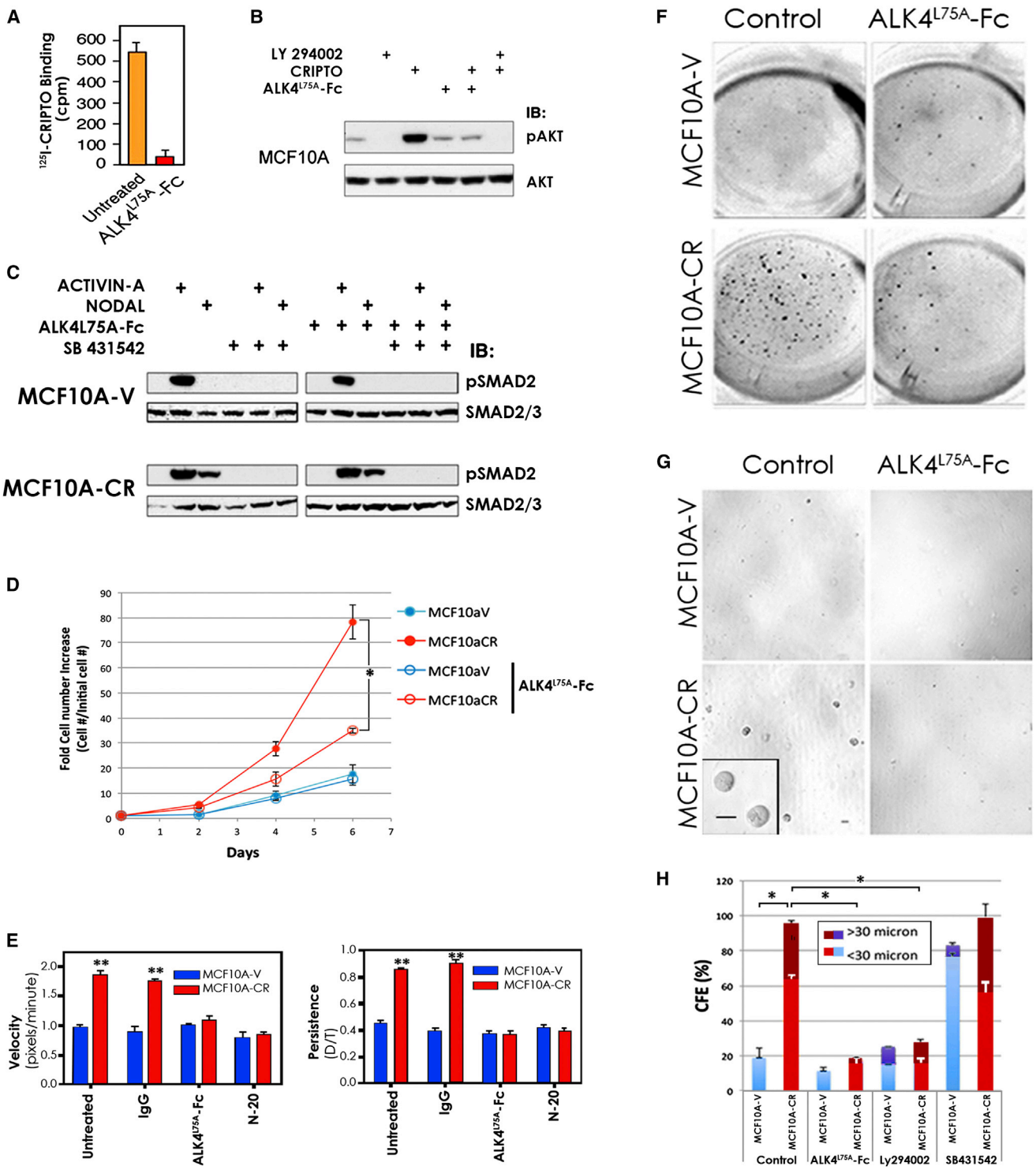

Figure 1. ALK4^{L75A}-Fc Inhibits Growth-Factor-like Effects of CRIPTO on Immortalized Human Mammary Epithelial Cells

(A) ALK4^{L75A}-Fc (10 μg/ml) inhibits binding of ^{125}I-CRIPTO to native MCF10A cells. Data from one of two independent experiments using three technical replicates are shown, with SDs.

(B) Phospho-AKT (Ser 473) or total AKT western blots on lysates from MCF10A cells treated with soluble CRIPTO (300 ng/ml), ALK4^{L75A}-Fc, and PI3K inhibitor LY 294002 (10 μM) as indicated.

(legend continued on next page)

dynamically expressed during mammary gland development (Bianco et al., 2008; Kenney et al., 1995) and in breast cancer (Gong et al., 2007) but has not been previously examined in the context of MaSCs. CRIPTO promotes proliferation, invasion, and migration of mammary epithelial cell lines in vitro, whereas its overexpression in the mouse mammary gland promotes excessive ductal branching, hyperplasia, and latent tumor growth (Rangel et al., 2012). Although the relevant molecular and cellular mechanisms for these effects remain to be determined, CRIPTO impacts multiple signaling pathways associated with stem cells and oncogenesis, including transforming growth factor β (TGF-β), phosphatidylinositol 3-kinase (PI3K), WNT, and NOTCH (Rangel et al., 2012). Two distinct CRIPTO signaling activities have been best characterized: (1) a coreceptor function in which CRIPTO modulates signaling of TGF-β ligands such as NODAL that signal via SMAD2/3 activation and (2) a growth-factor-like activity in which soluble CRIPTO activates SRC/mitogen-activated protein kinase/PI3K pathways in a TGF-β pathway-independent manner (Bianco et al., 2002; Gray and Vale, 2012). Both of these signaling activities require CRIPTO binding to cell-surface GRP78, an HSP70 family member that localizes to the surfaces of stem cells and tumor cells (Gray and Vale, 2012; Kelber et al., 2009; Miharada et al., 2011; Shani et al., 2008).

Here, we investigate CRIPTO's ability to regulate primary fetal and adult mammary stem/progenitor cells using a series of ex vivo culture and mammary gland reconstitution experiments. We develop an antagonist that selectively blocks the growth factor-like signaling of soluble CRIPTO without affecting its cell-surface coreceptor activity, and we use this reagent to demonstrate that soluble CRIPTO maintains the MaSC state ex vivo. We further identify cell-surface GRP78 as a determinant of CRIPTO responsiveness and critical functional marker in fetal and adult MaSCs.

RESULTS

An ALK4-Based Antagonist Inhibits Growth-Factor-like Effects of Soluble CRIPTO on Mammary Epithelial Cells

We developed a CRIPTO antagonist in order to test if CRIPTO signaling is required for the maintenance of MaSCs. We took advantage of the CRIPTO binding properties of the extracellular domain (ECD) of the ACTIVIN/NODAL type I receptor ALK4 (Bianco et al., 2002; Gray and Vale, 2012; Yeo and Whitman, 2001) and the fact that a leucine to alanine substitution at amino acid 75 (L75A) disrupts ALK4/ACTIVIN binding without affecting ALK4 binding to CRIPTO (Kelber et al., 2008). Although the L75A mutation does not guarantee complete specificity of ALK4 ECD binding to CRIPTO, we reasoned that this substitution should increase the selectivity of their interaction. We previously showed that a kinase-deleted ALK4^{L75A} protein blocks CRIPTO effects on ACTIVIN and NODAL signaling (Kelber et al., 2008), leading us to hypothesize that a soluble version of the ALK4^{L75A} ECD would similarly block CRIPTO signaling. To test this, we fused an N-terminally Flag-tagged ALK4-ECD^{L75A} to the Fc region of human immunoglobulin G (ALK4^{L75A}-Fc). We purified the recombinant protein from conditioned media using affinity chromatography and confirmed its ability to bind CRIPTO in solution (Figures S1A–S1D and Supplemental Experimental Procedures available online).

Using the CRIPTO-responsive human mammary epithelial MCF10A cell line, we find that ALK4^{L75A}-Fc effectively inhibits binding of soluble CRIPTO to intact cells and blocks CRIPTO-dependent augmentation of AKT phosphorylation (Figures 1A and 1B). This effect appears to be specific, because ALK4^{L75A}-Fc only blocks CRIPTO-dependent AKT phosphorylation, whereas a PI3K inhibitor (LY 294002) blocks detection of both CRIPTO-induced and basal phospho-AKT (Figure 1B). As expected, and in

(C) Phospho-SMAD2 and SMAD2/3 western blots on MCF10A cells stably transduced with CRIPTO-Flag virus (MCF10A-CR) or control virus (MCF10A-V) and treated as indicated with ACTIVIN A (1 nM), NODAL (30 nM), ALK4^{L75A}-Fc, and the ALK4/5/7 inhibitor SB 431542 (10 μM).
(D) Time course showing that MCF10A-CR cells accumulate more rapidly than MCF10A-V cells in 2D culture. Treatment with ALK4^{L75A}-Fc selectively inhibits growth of MCF10A-CR cells. *$p < 0.01$. Triplicate wells in a representative experiment are shown, with SDs.
(E) MCF10A-CR cells are more migratory than MCF10A-V cells. The CRIPTO-dependent increase in migrational velocity and persistence is blocked by ALK4^{L75A}-Fc treatment or a GRP78 neutralizing antibody (N-20). **$p < 0.01$, two-way ANOVA. Data from $\geq$50 individual cells from three fields of view per condition in one experiment (of two performed) are shown, with SDs.
(F) Suspension cultures of MCF10A-V and MCF10A-CR cells 11 days after seeding in 24-well plates. MCF10A-CR cells grow more rapidly than MCF10A-V cells in suspension culture, and this growth advantage is inhibited by ALK4^{L75A}-Fc treatment.
(G) MCF10A-CR cells produce larger and more plentiful colonies than MCF10A-V cells when grown in immobilizing methylcellulose suspension cultures, and ALK4^{L75A}-Fc treatment blocks this CRIPTO-dependent growth. Bar represents 30 μm.
(H) Colony growth was significantly reduced by either ALK4^{L75A}-Fc treatment or PI3K inhibition (LY 294002 10 μM), but not by treatment with SB 431542. *$p < 0.05$. Two independent experiments with duplicate wells in each are tabulated, with SDs. SB 431542 treatment increased colony number, but not mean size, of MCF10A-V cells.
See also Figures S1 and S2.

contrast to CRIPTO-independent ACTIVIN A signaling, NODAL treatment induces SMAD2 phosphorylation in MCF10A cells stably transduced with CRIPTO lentivirus (MCF10A-CR), but not in control cells transduced with empty vector (MCF10A-V) (Figure 1C). Both NODAL and ACTIVIN A signal via ALK4, and SMAD2 phosphorylation in response to each ligand is blocked by the ALK4/5/7 kinase inhibitor SB 431542 (Figure 1C). ALK4^{L75A}-Fc treatment, on the other hand, has no effect on ACTIVIN A-induced SMAD2 phosphorylation (Figure 1C), consistent with our previous demonstration that the ALK4^{L75A} mutation blocks ACTIVIN A binding (Kelber et al., 2008). Surprisingly, however, ALK4^{L75A}-Fc treatment also has no discernible effect on CRIPTO-dependent NODAL signaling in MCF10A-CR cells (Figure 1C) or on CRIPTO-dependent NODAL induction of a SMAD2-responsive luciferase reporter in 293T cells (Figure S1E). This failure of ALK4^{L75A}-Fc to block CRIPTO coreceptor activity is consistent with our inability to detect ALK4^{L75A}-Fc binding on the surface of intact CRIPTO-overexpressing 293T cells (Figure S1F).

MCF10A-CR cells secrete CRIPTO (Figure S2A) and have elevated levels of PI3K/AKT signaling relative to MCF10A-V cells (Figure S2B), leading us to test if ALK4^{L75A}-Fc inhibits autocrine/paracrine CRIPTO growth factor activity in these cells. We use live-cell time-course and time-lapse microscopy, respectively, to track proliferation and migration of MCF10A-CR cells and control cells (MCF10A-V). MCF10A-CR cells accumulate more rapidly than MCF10A-V cells (Figure 1D), consistent with our previous findings (Kelber et al., 2009), and these CRIPTO expressing cells also have enhanced migration relative to control cells (Figure 1E). Treatment with ALK4^{L75A}-Fc inhibits the CRIPTO-dependent increases in growth (Figure 1D) and motility (Figure 1E; Figure S2C; Movies S1, S2, S3, and S4). The inhibitory effects of ALK4^{L75A}-Fc treatment on CRIPTO-dependent migrational velocity and persistence are similar to those of GRP78 antibody (N-20) (Figure 1E; Figure S2C) that we previously showed blocks CRIPTO/GRP78 binding (Kelber et al., 2009).

We also analyzed the effects of CRIPTO signaling and antagonism on MCF10A cells in 3D culture in the presence or absence of the reconstituted basement membrane Matrigel. Although suspension cultures have been widely used to measure the production of multicellular mammary epithelial structures called "mammospheres" (Dontu et al., 2003), Matrigel-containing mammary epithelial cultures promote the formation of differentiated, polarized acinar structures from MCF10A cells and multilayered, multilineage organoids from primary mammary epithelial stem cells (Debnath et al., 2003; Spike et al., 2012). MCF10A-CR cells accumulate more rapidly than MCF10A-V cells in free-floating suspension cultures, where they exhibit a greater proportion of cells with 2N-4N DNA content indicative of cycling S phase cells (Figure 1F; Figures S2D and S2E). The growth promoting effects of CRIPTO under these conditions are blocked by treatment with ALK4^{L75A}-Fc or LY 294002, but not SB 431542 (Figure S2D). We used methylcellulose immobilization of cells in suspension cultures to measure the size of individual spheres (Figures 1G and 1H). Consistent with the increased cell numbers observed in free-floating cultures, immobilized MCF10A-CR cells form larger, more numerous mammospheres than MCF10A-V cells, and the increased growth of the CRIPTO-expressing cells is again blocked by ALK4^{L75A}-Fc and LY 294002, but not by SB 431542 (Figure 1H). CRIPTO overexpression similarly promotes MCF10A colony growth in Matrigel, and this is inhibited by treatment with ALK4^{L75A}-Fc, whereas treatment of these cultures with NODAL neither augments CRIPTO-induced growth nor overcomes ALK4^{L75A}-Fc -mediated inhibition of CRIPTO-induced growth (Figure S2F). Altogether, these results indicate that soluble CRIPTO promotes proliferation and migration of mammary epithelial cells and that this can be blocked by ALK4^{L75A}-Fc.

CRIPTO/GRP78 Expression and Function in fMaSCs

Our data show that MCF10A cells respond to soluble CRIPTO signaling in multiple contexts, including 3D growth assays that are similar to those used previously to evaluate stem cell-like cellular behaviors (Dontu et al., 2003). We also previously demonstrated that soluble CRIPTO activates the PI3K/AKT pathway in MCF10A cells by binding to cell-surface GRP78 (Kelber et al., 2009). These findings, together with reports that CRIPTO and GRP78 cooperatively regulate stem cell function in other contexts, prompted us to test if CRIPTO and GRP78 are expressed in murine mammary tissue and if the CRIPTO/GRP78 pathway is operative in primary mammary stem/progenitor cells. We first investigated the pattern of CRIPTO and GRP78 expression in embryonic day 18.5 (E18.5) mouse mammary rudiments, because they provide a rich source of robust stem cell activity (Spike et al., 2012). We find GRP78 to be expressed throughout the mammary rudiment, with the most intense and distinct staining coinciding with the burgeoning, arborized mammary epithelium, demarcated here by costaining with antibodies to KRT8 (Figures 2A and 2B). By contrast, CRIPTO staining is more diffuse and distributed throughout the rudiment, with significant staining in the fetal mammary stroma and areas within and adjacent to the GRP78-positive and KRT8-positive epithelium. Interestingly, we observe intense CRIPTO staining at or near the termini of the arborized mammary rudiment, where it overlaps with both the condensed mesenchyme adjacent to the epithelium and epithelial cells that stain prominently for

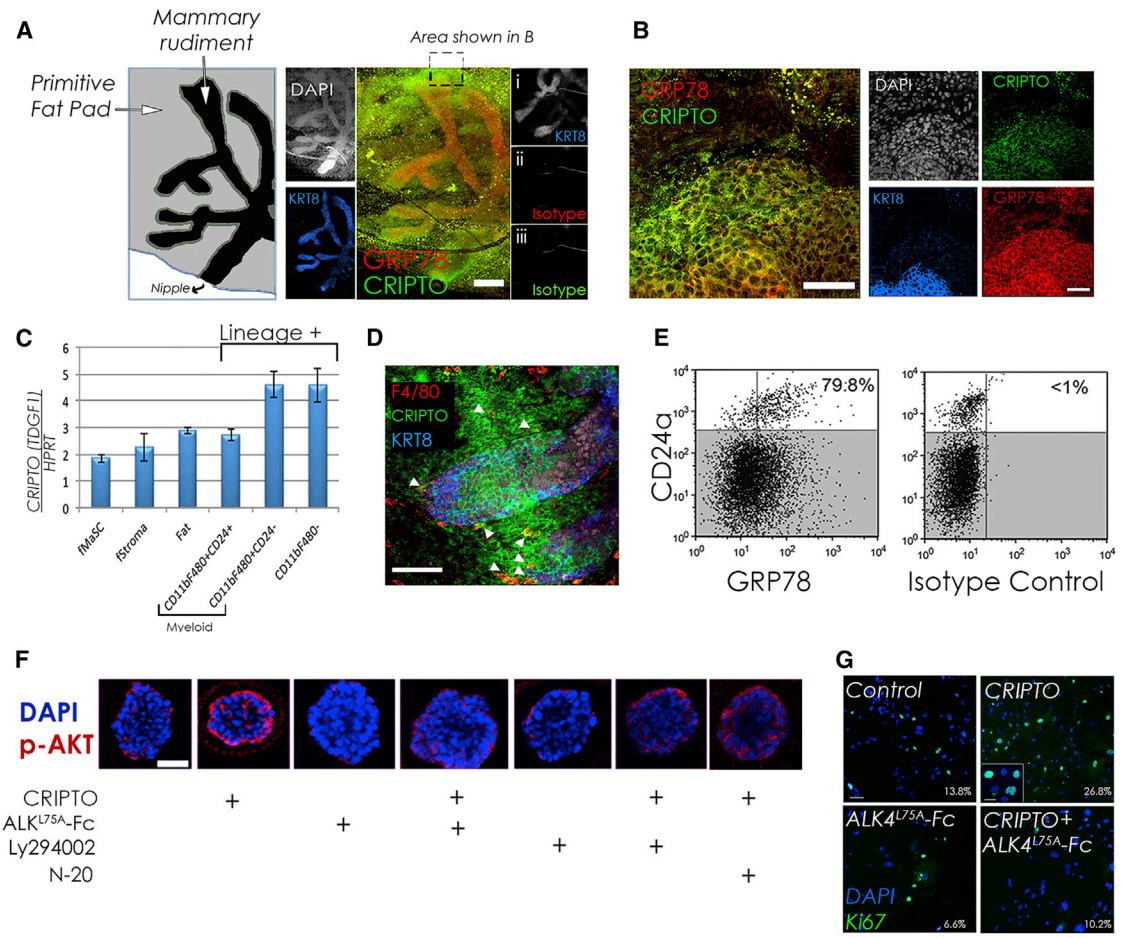

Figure 2. Expression of CRIPTO and GRP78 in the Fetal Mammary Rudiment and Responsiveness of fMaSCs to Soluble CRIPTO

(A and B) Whole-mount E18.5 fetal mammary rudiment demarcated with immunofluorescence staining for KRT8 (blue) or DAPI (white) and costained for CRIPTO (green) and GRP78 (red) (right). (A, i–iii) control rudiment stained with KRT8 and isotype-matched controls for GRP78 and CRIPTO. Scale bar represents 200 μm (A) or 50 μm (B).

(C) CRIPTO is expressed in the fMaSC population and stromal cells as measured by RT-PCR. A total of 150 rudiments were pooled and assayed in technical triplicates, with SDs.

(D) CRIPTO staining colocalizes with F4/80 staining (arrows) adjacent to mammary epithelium demarcated by KRT8 staining (blue).

(E) Flow cytometric analysis of fetal mouse mammary cells stained with CD24, GRP78, and isotype control antibodies as indicated. The percentage of the CD24^{high} population also positive for GRP78 is shown.

(F) Phospho-AKT staining in serum-starved, fMaSC-derived organoids treated as indicated with soluble CRIPTO (300 ng/ml), ALK4^{L75A}-Fc (10 μg/ml), LY 294002 (10 μM), or N-20 (2 μg/ml). Scale bar represents 50 μm.

(G) 2D fMaSC cultures were treated with CRIPTO (400 ng/ml) and/or ALK4^{L75A}-Fc (10 μg/ml) as indicated and stained with Ki67 antibody and DAPI. Scale bar represents 50 μm, and inset represents 10 μm.

GRP78 (Figures 2A and 2B). *CRIPTO* mRNA was detected in fMaSCs but is more highly expressed in a variety of other cell populations isolated from the fetal mammary microenvironment, including putative adipose precursor cells that resist centrifugation during rudiment processing ("Fat"), myeloid cells (Lin$^+$CD11b$^+$F4/80$^+$), and non-myeloid lineage-positive cells (CD11b$^-$F4/80$^-$) (Figure 2C). *CRIPTO* message is also present in other stromal cells (fStromal; Lin$^-$CD24^{low}) that likely include mammary tissue fibroblasts (Figure 2C). Costaining of the mammary rudiment for the macrophage marker F4/80 confirms colocalization of CRIPTO protein with not only macrophages but also other nonmacrophage stromal components adjacent to the fetal mammary epithelium (Figure 2D). Thus, CRIPTO is expressed in multiple cell types within the MaSC microenvironment, leading us to reason that soluble secreted CRIPTO may govern fMaSC behavior as an autocrine/paracrine growth factor.

Our previous studies indicating that CRIPTO signals via cell-surface GRP78 led us to test if GRP78 is expressed on the surface of fMaSCs ($Lin^{-}CD24^{high}$) and if these cells respond to soluble CRIPTO in a GRP78-dependent manner. We analyzed dissociated cells from E18.5 mammary rudiments by flow cytometry and discovered that >80% of the fMaSC population is GRP78 positive (Figure 2E). Furthermore, when we treat fMaSC-derived Matrigel colonies with soluble CRIPTO, we observe increased AKT phosphorylation that is blocked by treatment with $ALK4^{L75A}$-Fc or LY 294002 (Figure 2F). This increase in AKT phosphorylation is also blocked by N-20, indicating that CRIPTO signals via cell-surface GRP78 in these cells (Figure 2F). Soluble CRIPTO treatment also increases the proportion of $Ki67^{+}$ cells relative to untreated cells in 2D culture, and this effect was once again blocked by $ALK4^{L75A}$-Fc treatment (Figure 2G). Thus, multiple cell types within the fetal mammary rudiment produce CRIPTO, and it can act on cells within the fMaSC population.

CRIPTO/GRP78 Signaling Promotes Maintenance of fMaSCs Ex Vivo

To explore the consequences of CRIPTO signaling in MaSCs further, we examined its effects on growth, self-renewal, and differentiation in fMaSC cultures. We previously reported that fMaSCs grown in media that promotes their differentiation give rise to a high proportion of bilineage organoids containing both $KRT8^{+}KRT14^{-}$ luminal cells and $KRT14^{+}KRT8^{-}$ myoepithelial cells by 7–12 days of culture (Spike et al., 2012). At 5 days of culture, organoids grown in this differentiation promoting media typically contain a fraction of cells coexpressing KRT8 and KRT14 (Figure 3A, top left, yellow arrows, and Figure 3B). Supplementation of these cultures with CRIPTO or $ALK4^{L75A}$-Fc has opposing effects on the fraction of organoids containing double-positive ($KRT8^{+}KRT14^{+}$) cells and on the amount of double-positive area per organoid (Figure 3A, left panels, and Figure 3B; Figures S3A and S3B). Specifically, CRIPTO treatment increases the proportion of double-positive area per organoid while $ALK4^{L75A}$-Fc treatment decreases it, suggesting that CRIPTO signaling promotes maintenance of a multipotent phenotype. However, rapid cellular differentiation under these culture conditions prevented us from confirming stem cell activity of resultant colonies by mammary reconstitution analyses (data not shown; Spike et al., 2012).

To address this issue, we developed culture conditions that are better able to produce mammary epithelial colonies including bilineage organoids that also give rise to mammary outgrowths following transplantation. CRIPTO and $ALK4^{L75A}$-Fc also have opposite effects on the stem cell phenotype of fMaSC-derived colonies grown in this stem cell maintenance media (Figure 3A, right panels, and Figure 3B). Endogenous CRIPTO is implicated as a stem cell factor in these cultures by the fact that $ALK4^{L75A}$-Fc treatment alone increases the number of keratin single-positive cells discernible per organoid (Figure 3A, right panels, red arrows). $ALK4^{L75A}$-Fc also significantly increases the amount of single keratin staining area (either $KRT14^{+}KRT8^{-}$ or $KRT8^{+}KRT14^{-}$) relative to $KRT8^{+}KRT14^{+}$ double-positive area per organoid (Figure 3B; Figure S3B), although some double-positive cells are evident in all organoids in maintenance media following 5 days of culture (Figures 3A and 3B; Figure S3B).

Although our data indicate that CRIPTO signaling correlates with KRT8+KRT14+ double positivity, the precise relationship between keratin expression and differentiation status in these cultures is uncertain. It is therefore important that CRIPTO signaling also has *functional* stem cell relevance, because treatment with soluble CRIPTO enhanced the ability of fMaSC-derived colonies grown for 5 days in this media to reconstitute mammary glands upon transplantation relative to untreated controls and this CRIPTO effect was attenuated by $ALK4^{L75A}$-Fc (Figure 3C). Despite the clear effects of CRIPTO signaling on keratin expression and transplantation, treatment with CRIPTO and/or $ALK4^{L75A}$-Fc does not significantly affect overall colony number and size in 5-day cultures (Figure 3D). However, when cells are serially passaged for three rounds under stem cell maintenance conditions, $ALK4^{L75A}$-Fc treatment substantially reduces colony-forming efficiency and the growth of large colonies (>100 μm) is almost completely abolished (Figure 3D). Conversely, addition of CRIPTO can support a round of serial passage of fMaSC-derived cells, even under conditions that strongly favor differentiation (Figure 3D). We note that clonogenicity of fetal mammary cells was recently shown to be enhanced by unidentified factors secreted by 3T3 fibroblasts in coculture (Makarem et al., 2013). We find that 3T3 cells express CRIPTO protein (Figure S3D) and that their ability to enhance clonogenicity of fetal mammary cells in coculture can be partially blocked by treatment with either $ALK4^{L75A}$-Fc or CRIPTO antibodies (Figure S3E). This result is consistent with our results using recombinant proteins and further highlights the potential for non-cell-autonomous CRIPTO regulation of fMaSCs.

GRP78 Is a Critical Functional Marker and Cell-Surface Determinant of CRIPTO-Responsive MaSCs

We examined CRIPTO and GRP78 expression in the adult mammary gland and identified marked immunoreactivity for both proteins that overlaps with the morphologically distinct mammary ductal epithelium and adjacent adipose tissue (Figure 4A). Immunofluorescent colocalization studies confirm overlapping CRIPTO and GRP78 staining

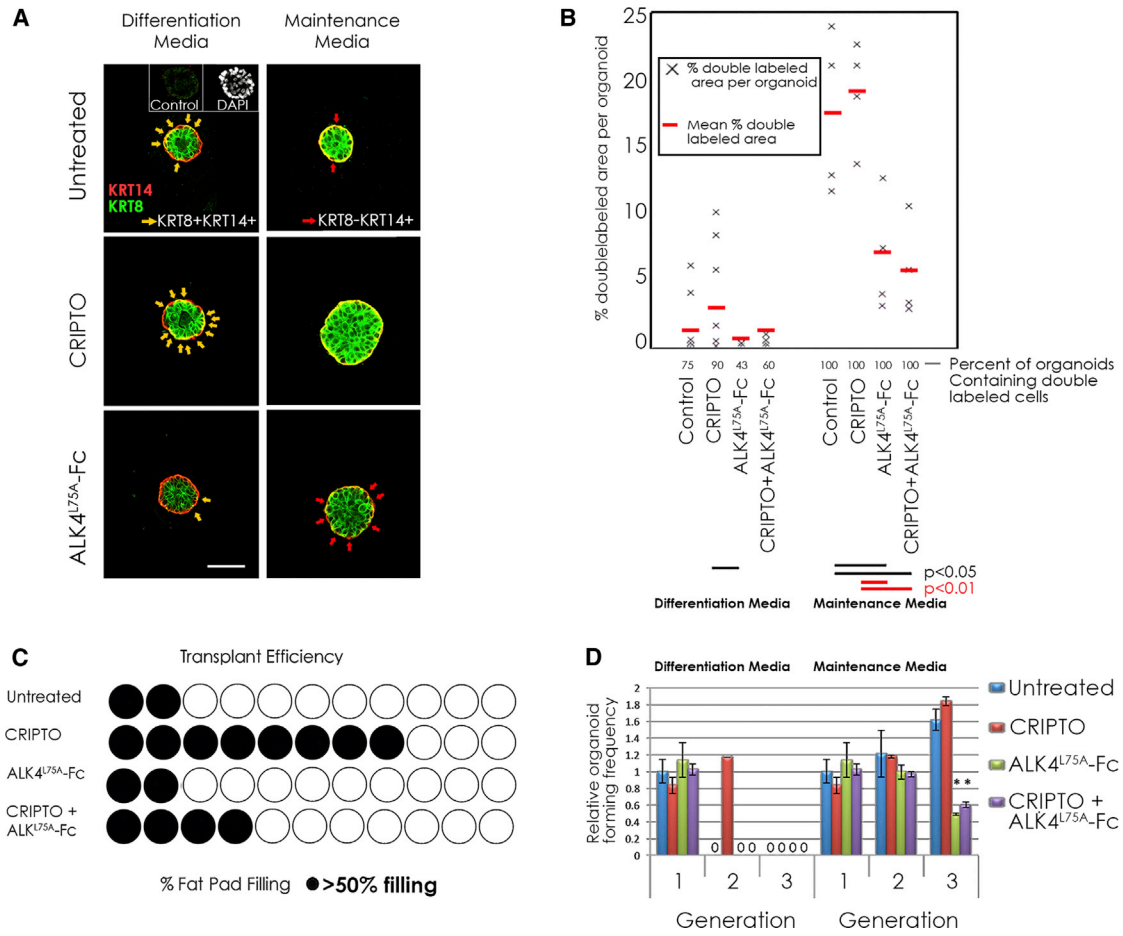

Figure 3. CRIPTO Promotes Maintenance of fMaSCs

(A) Sphere-bisecting confocal cross sections of day 5, fMaSC-derived colonies grown in Matrigel and stained with KRT8 (green) and KRT14 (red). Colonies were grown in differentiation media or maintenance media with soluble CRIPTO (0.33 μg/ml) or ALK4^{L75A}-Fc (10 μg/ml) as indicated. Yellow arrows indicate KRT8^{+}KRT14^{+} double-positive cells. Red arrows indicate lineage-committed KRT14 single-positive cells. Control represents the same isotype. Scale bar represents 100 μm.

(B) KRT8 and KRT14 staining was quantified from images and is represented as the percent KRT8^{+}KRT14^{+} double-labeled area per organoid. The percentage of organoids containing KRT8^{+}KRT14^{+} double-labeled cells is also indicated. Results of three independent representative experiments are shown.

(C) Mammary gland repopulation efficiency of first-generation colonies grown in Matrigel-containing maintenance media culture with soluble CRIPTO and/or ALK4^{L75A}-Fc. Each circle represents one recipient mammary gland. Shaded circles represent ducts extending through >50% of the fat pad.

(D) Colony-forming efficiencies (>100 μm) at first, second, and third passage for fMaSCs grown for 7 days per passage in differentiation or maintenance media with CRIPTO and/or ALK4^{L75A}-Fc. Results of three independent experiments (maintenance media) and a representative experiment (differentiation media) were quantified. Triplicate wells were quantified in each. Error bars represent SDs. *p $\leq$ 0.01. See also Figure S3.

in these cell types, including elevated staining in adipose and a subset of mammary epithelial cells (Figure 4B). To determine whether adult MaSCs require GRP78, we used CRE-mediated recombination and excision of GRP78 alleles together with mammary gland reconstitution experiments. In these experiments, cells harboring CRE-expressing virus failed to reconstitute mammary ductal trees in each of nine transplant attempts (zero out of nine), while an equivalent number of cells transduced with control virus robustly repopulate the gland (three out of three) (Figure 4A). Furthermore, cells isolated from control outgrowths exhibit cell-surface GRP78 and contain both the luminal and myoepithelial fractions (Figure S4C). In contrast, we only occasionally recover a low number of presumptive mammary epithelial cells from transplants of GRP78Fl/Fl cells infected with CRE virus. These cells

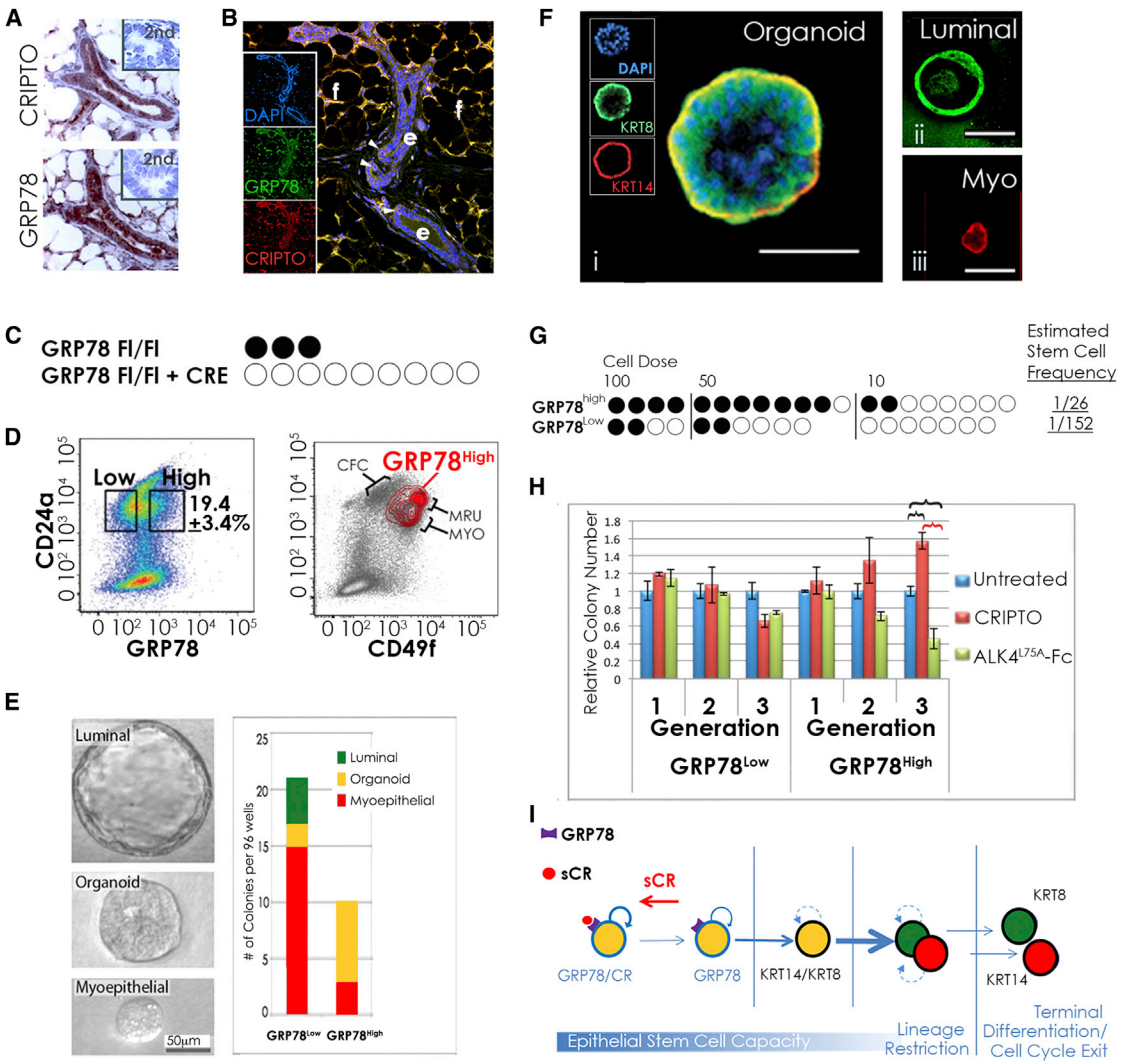

Figure 4. GRP78 Is Required for MaSC Activity and Marks a CRIPTO-Responsive Stem Cell-Enriched Population of Adult Mouse Mammary Epithelial Cells

(A) Immunohistochemical localization of CRIPTO and GRP78 in adult mouse mammary tissue. Inset: secondary antibody alone (2^{nd}).

(B) CRIPTO and GRP78 proteins colocalize in stromal areas including adipose (f, fat) and in epithelial structures (e), where a subset of cells display elevated staining for both markers (white arrows).

(C) Repopulation rate of de-epithelialized mammary glands inoculated with 500 GRP78-floxed epithelial cells transduced with Ad-CRE/GFP- or Ad-GFP and sorted for GFP. Each circle represents one recipient mammary gland. Filled circles indicate >50% fat pad filling.

(D) Flow cytometric analysis of wild-type adult mouse mammary cells stained for CD24 and GRP78 (lineage excluded) indicating the presence of cell-surface GRP78 in adult mammary epithelia and demarcating the $GRP78^{high}$ and $GRP78^{low}$ populations (left). Antibodies to CD49f were also incorporated (right), and cells positive for GRP78 and CD24 were gated to generate a population density graph (red lines) superimposed on the CD24/CD49f staining. The standard positions of the CFC, MYO, and MRU populations (Stingl et al., 2006) are indicated.

(E) Colonies grown from single cells sorted into individual wells in 96-well plates. Luminal, organoid, and myoepithelial morphologies were distinguishable (left). The number of each type of clonal outgrowth deriving from single $GRP78^{low}$ and $GRP78^{high}$ cells in one representative experiment (of three similar experiments) was quantified according to morphology (right).

(F) Confocal micrographs showing the keratin distribution observed in representative colonies grown from cells sorted using CD24 and GRP78. $GRP78^{low}$ cells predominantly expressed either KRT8 or KRT14, while $GRP78^{high}$ cultures frequently exhibited $KRT8^{+}KRT14^{+}$ outgrowths. Representative organoid (i), luminal (ii), and myoepithelial (iii) colonies are shown. Color panels show individual fluorophores separately for the organoid (i, insets). Scale bars represent 100 μm.

(legend continued on next page)

appear restricted to the mature luminal fraction, lack detectable cell-surface GRP78, and do not give rise to colonies when cultured in vitro (Figure S4A; data not shown). These data indicate that GRP78 is required for MaSC activity as measured by transplantation assays.

Next, we sought to examine the role of cell-surface GRP78 as an adult MaSC marker and as a MaSC regulator specifically in its capacity as a mediator of CRIPTO signaling. We isolated CD24-positive mammary epithelial cells with either high ($GRP78^{high}$) or low ($GRP78^{low}$) levels of cell-surface GRP78 from wild-type mice (Figure 4D, left panel). A substantial portion of adult mammary epithelial cells was $GRP78^{high}$ (19.4% ± 3.4% of the CD24-positive fraction), though the proportion was considerably lower than in fetal mammary epithelia (Figure 3D). In costained samples, we observe that while the $GRP78^{high}$ population overlaps partially with the previously reported luminal colony-forming cell (CFC) and myoepithelial (MYO) populations, it overlaps most precisely with the stem cell-enriched $CD24^{med}CD49f^{high}$ mammary repopulating unit (MRU) fraction (Figure 4D, right panel) (Stingl et al., 2006). While cells from both the $GRP78^{high}$ and $GRP78^{low}$ fractions produce clonal outgrowths in Matrigel culture, those derived from the $GRP78^{high}$ population are much more likely to give rise to colonies containing multiple cell layers (Figure 4E; organoids) and to stain positive for both KRT14 and KRT8 (Figure 4F; Figure S4B). In these assays, the most frequently observed and morphologically distinguishable colony types include those that appear luminal, composed of a single peripheral cell layer surrounding an open lumen, small myoepithelial colonies (usually < 16 cells), and distinctive, multilayered organoids containing both luminal and myoepithelial cell types (Figures 4E and 4F) (Spike et al., 2012; Stingl et al., 2006). Importantly, these morphologically distinct colony types are produced in cultures both when single cells were plated in individual wells (Figure 4E) and when cells are plated at single-cell densities (1,000 cells per 0.32 cm^2) (Figure 4F; data not shown) (Spike et al., 2012). Thus, the substantially higher proportion of organoids and $KRT14^+KRT8^+$ double-positive colonies formed from the $GRP78^{high}$ population (Figures 4E and 4F; Figure S4B) suggests that the $GRP78^{high}$ population is enriched for bipotent stem/progenitor cells. In contrast, $GRP78^{low}$ cells predominantly give rise to small myoepithelial ($KRT14^+KRT8^-$) or monolayered luminal ($KRT14^-KRT8^+$) outgrowths (Figures 4E and 4F; Figure S4B).

As an independent criterion for assessing the stem cell content of the $GRP78^{high}$ population, we transplanted $CD24^{med}GRP78^{high}$ and $CD24^{med}GRP78^{low}$ mammary epithelial cell populations into cleared mammary fat pads at limiting dilutions. The results clearly indicate that the $CD24^{med}GRP78^{high}$ cells reconstitute mammary glands more efficiently the $CD24^{med}GRP78^{low}$ cells (Figure 4G; Figures S4C–S4E). We estimate the frequency of mammary gland-reconstituting units to be approximately 1/26 in the $GRP78^{high}$ cells (90% confidence interval [CI], 1/15–45.4; extreme limiting dilution analysis [ELDA]) versus approximately 1/152 in the $GRP78^{low}$ population (90% CI, 1/67.0–346.2; ELDA) (Figure 4G; Figure S4E). This correlates with a significant enrichment ($p < 0.01$; ELDA) of stem cell activity in the $GRP78^{high}$ fraction relative to the $GRP78^{low}$ cells (Figure 4G; Figures S4C–S4E). Outgrowths from transplanted $GRP78^{high}$ cells resemble endogenous mammary glands in FACS analyses including the presence of $GRP78^{high}$ cells within the CD24 expressing mammary epithelium (Figure S4F). Significantly, the self-renewal potential of these cells is evident in their capacity to reconstitute fully arborized mammary epithelial outgrowths in tertiary transplants that respond normally to pregnancy (Figure S4G). We also identify a diffuse, small, and variable population of GRP78 "superpositive" ($GRP78^{high+}$) cells with intermediate performance in stem cell assays (Figures S4D and S4E).

Because CRIPTO signaling promotes serial passage of fMaSCs ex vivo (Figure 3D), we tested the effects of this pathway on cultures of adult $GRP78^{high}$ and $GRP78^{low}$ mammary epithelial populations. Consistent with its greater enrichment for cells with a bipotent stem cell phenotype (Figures 4E–4G; Figure S4B), the $GRP78^{high}$ population exhibits greatly enhanced potential for serial colony formation relative to $GRP78^{low}$ cells, especially over increasing serial passage number in Matrigel (Figure 4H; Figure S4H). Furthermore, serial passage of $GRP78^{high}$ cells is significantly enhanced by CRIPTO treatment (Figure 4H) and, similar to what was observed with fMaSCs, serial colony formation of adult $GRP78^{high}$ cells is also inhibited by $ALK4^{L75A}$-Fc treatment, suggesting that endogenous

(G) Mammary gland repopulation efficiencies of $GRP78^{high}$ and $GRP78^{low}$ cells represented as in (C) (the data fit a single-hit model; likelihood ratio test $p = 0.938$; ELDA).
(H) $GRP78^{high}$ cells are selectively responsive to soluble CRIPTO or $ALK4^{L75A}$–Fc treatment when serially passaged in Matrigel culture. Results of two independent experiments conducted in triplicate are shown, with SDs. Black bracket $p < 0.05$; red bracket $p < 0.01$.
(I) Model depicting cooperativity of soluble CRIPTO (sCR) and cell-surface GRP78 in promoting mammary stem cell maintenance. Soluble CRIPTO reinforces a robust primitive epithelial stem cell state, whereas loss of soluble CRIPTO signaling leaves cells vulnerable to differentiation cues and eventual loss of stem cell characteristics such as bipotency (yellow cells) and self-renewal (circular arrow).
See also Figure S4.

soluble CRIPTO maintains the self-renewal potential of these cells. By contrast, GRP78^{low} cells are largely refractory to treatment with CRIPTO or ALK4^{L75A}-Fc (Figure 4H), consistent with a requirement for surface GRP78 for CRIPTO signaling (Kelber et al., 2009). Together, these data support a role for soluble CRIPTO in maintaining the stem cell phenotype of GRP78^{high} mammary epithelial cells.

The data are consistent with a model (Figure 4I) in which surface GRP78 is a functional MaSC marker. In this model, the most undifferentiated MaSC state depends on endogenous CRIPTO signaling, because treatment with ALK4^{L75A}-Fc leads to loss of multipotency and eventual rundown of self-renewal in serial passage. In addition, a subset of cells, at least in the adult context, lacks endogenous CRIPTO but can respond to exogenous soluble CRIPTO with increased serial clonogenicity or self-renewal. Thus, according to this model, CRIPTO treatment shifts cells to a more primitive, stable, or competent stem cell state while ALK4^{L75A}-Fc treatment makes them susceptible to commitment and differentiation.

DISCUSSION

Extracellular signaling factors play critical roles in regulating the balance between stem cell self-renewal and differentiation (Jones and Wagers, 2008; Spradling et al., 2001). In the present study, we identify CRIPTO as one such factor that promotes multipotency and maintains gland reconstitution potential of mammary stem/progenitor cells ex vivo. We also show that the CRIPTO cell-surface receptor GRP78 is required for MaSC activity and CRIPTO responsiveness. Thus, CRIPTO and GRP78 are shared determinants of both fetal and adult mammary stem/progenitor cells pointing to a developmentally conserved role for the CRIPTO/GRP78 pathway in maintenance of the MaSC state.

ALK4^{L75A}-Fc Identifies Soluble CRIPTO as a MaSC Factor

ALK4^{L75A}-Fc selectively targets soluble CRIPTO and blocks CRIPTO-induced PI3K/AKT signaling, indicating that CRIPTO's growth factor-like activity is essential for maintenance of MaSC properties in the contexts we analyzed. Miharada et al. (2011) similarly showed that soluble CRIPTO regulates hematopoietic stem cells (HSC) via the PI3K/AKT pathway independent of SMAD2/3 signaling. However, although our results uncover a critical role for soluble CRIPTO growth-factor-like signaling in regulating MaSC behavior, they do not exclude a role for CRIPTO coreceptor function. Indeed, NODAL, which requires CRIPTO or a related coreceptor, may act on fMaSCs during development in vivo, because it is expressed in fetal mammary stroma (Spike et al., 2012).

ALK4^{L75A}-Fc treatment alone is sufficient to cause MaSC differentiation and loss of self-renewal potential ex vivo, suggesting that endogenously secreted CRIPTO sustains the clonogenicity and multipotency of mammary epithelial cells in maintenance media and in 3T3 fibroblast cocultures. Consistent with this, CRIPTO treatment inhibits lineage commitment of cells in organoid culture and increases their serial colony formation and transplantation capacity. Therefore, CRIPTO acts as an extrinsic, soluble regulator of MaSC function in vitro, raising the possibility that it may function similarly as an autocrine/paracrine stem cell factor in vivo. In support of such a role, we show that GRP78 is prominently expressed throughout the ductal epithelium within the fetal mammary rudiment while CRIPTO is concentrated near the termini of the epithelial tree and the mesenchyme surrounding these termini where stem cell activity may be focused (Kenney et al., 2001). *CRIPTO* expression is low in fMaSCs but higher in a variety of nonepithelial cells of the mammary rudiment such as fat cells and macrophage/myeloid cells that could mark potential niche sources of secreted CRIPTO. Adipose tissue has been previously reported to express CRIPTO (Andersson et al., 2008) and constitutes the natural environment for growth and development of the mammary ductal epithelium (Veltmaat et al., 2003). Myeloid cells, including macrophages, may also provide soluble CRIPTO for stem cell regulation, because they comprise important niche components in other systems and are required for effective mammary reconstitution (Ehninger and Trumpp, 2011; Gyorki et al., 2009).

Cell-Surface GRP78 Is a Developmentally Conserved Marker of Fetal and Adult MaSCs

Our data identify cell-surface GRP78 as an enrichment marker of mammary stem/progenitor cells. CRIPTO and GRP78 are coexpressed in the adult mammary gland, and cell-surface GRP78 correlates with the stem cell-surface markers CD24 and CD49f (Stingl et al., 2006). Bipotent stem/progenitor cells, though rare in the adult gland, are relatively plentiful in the sorted GRP78^{high} population. GRP78^{high} cells are also selectively responsive to CRIPTO signaling, because CRIPTO and ALK4^{L75A}-Fc had opposing effects on their serial colony growth and neither treatment significantly affected the GRP78^{low} population. Interestingly, the percentage of GRP78^{high} cells is greater in the fetal than in the adult mammary gland, in agreement with the larger percentage of stem cells in the fetal mammary gland than in the adult (Spike et al., 2012). However, despite its ability to augment serial colony formation in cultures derived from GRP78^{high} adult cells, CRIPTO

treatment only has a modest effect on serial colony formation of fMaSCs in maintenance media. It is possible that CRIPTO growth-factor-like signaling is maximally activated in newly isolated fetal, but not adult, stem cells. This would explain the profound ability of the CRIPTO antagonist ALK4^{L75A}-Fc to inhibit fMaSC maintenance despite the lack of a more profound effect of CRIPTO treatment on these cells. This activity appears to be more rapidly lost in stronger differentiation-promoting contexts, unveiling a clear effect of exogenous CRIPTO in sustaining a limited capacity for serial passage.

CRIPTO/GRP78 Signaling as a General Regulator of the Stem Cell State

CRIPTO is an established regulator of embryonic stem cells and induced pluripotent stem cells (Bianco et al., 2010), whereas GRP78 is a necessary mediator of CRIPTO signaling in human embryonic stem cells (Kelber et al., 2009) and promotes survival and proliferation of the murine inner cell mass cells that are precursors of murine embryonic stem cells (Luo et al., 2006). In the adult, GRP78 was recently reported to be essential for maintenance of adult intestinal stem cells (Heijmans et al., 2013) and conditional deletion of GRP78 in the hematopoietic system suppressed PI3K activity and decreased HSC number (Wey et al., 2012a, 2012b). Furthermore, CRIPTO was shown to be a hypoxic niche-associated factor that maintains the stem cell state and transplantability of GRP78^{high} HSCs cultured ex vivo (Miharada et al., 2011). Although the mechanistic basis of CRIPTO/GRP78 signaling is still emerging, it has been shown that cell-surface localization of GRP78 often correlates with its overall expression level and occurs under stress conditions in which GRP78 is induced (Zhang et al., 2010). Therefore, although the stem cell niche remains poorly defined in the mammary gland, our results suggest that conditions known to increase the levels of GRP78 and/or CRIPTO such as hypoxia, nutrient deprivation, and endoplasmic reticulum stress could impact stem cell maintenance, expansion, and induction during normal mammary gland development and in homeostasis. Similarly, other signals from within the MaSC microenvironment likely intersect with CRIPTO and GRP78. For instance, Wnt signaling induces CRIPTO expression (Morkel et al., 2003) and has been reported to promote MaSC self-renewal in vitro (Zeng and Nusse, 2010).

Our recent demonstration that fMaSCs share a high degree of similarity with certain human breast cancers (Spike et al., 2012) is consistent with other evidence suggesting that tumor initiation, aggressiveness, and recurrence correlate with developmentally primitive states that are associated with cellular plasticity and increased stem cell disposition (Ben-Porath et al., 2008; Mizuno et al., 2010; Spike and Wahl, 2011). The results presented here show that CRIPTO/GRP78 signaling increases proliferation and maintains the potency of MaSCs ex vivo and raise the possibility that this pathway may be involved in promoting stem cell-like states in cancer, especially because expression of CRIPTO and GRP78 has been correlated with breast cancer progression and decreased patient survival (Dong et al., 2008; Gong et al., 2007; Lee, 2007). The stress-related cues that increase the expression of CRIPTO and GRP78 are prevalent in cancer and might specifically promote stem cell properties via increased CRIPTO/GRP78 signaling (Miharada et al., 2011; Zhang et al., 2010). In this regard, the ALK4^{L75A}-Fc CRIPTO antagonist described here would have potential as a stem cell-directed cancer therapeutic.

EXPERIMENTAL PROCEDURES

See Supplemental Information for additional details.

Reagents

ALK4^{L75A}-Fc was produced in 293T cells and purified by sequential protein-A and Flag affinity chromatography from conditioned media. Recombinant mouse CRIPTO (R&D Systems) was iodinated as previously described (Kelber et al., 2009). The following antibodies were used: CRIPTO (Abcam), GRP78 (N-20, Santa Cruz Biotechnology), KRT14 (AF-64, Covance), KRT8 (Troma-1, DSHB), F4/80 (BM8, eBioscience), Ki67 (B56, BD). Polyclonal rabbit antibodies directed against amino acids 19–39 of human GRP78 or amino acids 81–97 of mouse CRIPTO were produced in-house (see Supplemental Information). The A3-luciferase reporter assay has been described previously (Gray et al., 2003; Kelber et al., 2008). GRP78 floxed mice were provided by Amy Lee (University of Southern California).

Media

MCF10A media was composed of Dulbecco's modified Eagle's medium/F12 with 5% horse serum, 10 μg/ml insulin, 20 ng/ml epidermal growth factor, 100 ng/ml cholera toxin, 0.5 μg/ml hydrocortisone, and 10 μg/ml ciprofloxacin. Maintenance media was composed of MCF10A with 1× B27 supplement (Invitrogen). Differentiation media was composed of Epicult-B mouse media containing B supplement (Stem Cell Technologies), recombinant human epidermal growth factor, recombinant human basic fibroblast growth factor, and heparin, as previously described (Spike et al., 2012), with ciprofloxacin 10 μg/ml.

Cell Preparation and Culture

All animal care and procedures were approved and monitored by an Institutional Animal Care and Use Committee. MCF10A cells were cultured free floating in CnT-27 media or immobilized in MCF10A media with 2% Matrigel or 1% methylcellulose. Primary cells were prepared, sorted, cultured, and stained as previously described (Spike et al., 2012) using the indicated media. 3T3 cocultures were adapted from Makarem et al. (2013).

Assays

Proliferation in 2D was quantified on a Celigo microplate cytometer (Cyntellect). Migrational dynamics were tracked using time-lapse microscopy and Metamorph Imaging software on 2D cultures on Matrigel. DNA content was measured by Hoechst staining. mRNA abundance was measured using Superscript III (Life Technologies) and TaqMan assays Mm03024051_g1 and Mm01324427_m1 (Applied Biosciences). Mammary transplantation analyses were conducted as previously described (Spike et al., 2012). Organoid transplants used 20 organoids each by dilution. Western blotting and quantitation of cell-surface proteins by intact cell ELISA have also been previously described (Gray et al., 2003; Kelber et al., 2008).

Statistics

Data are presented as means and SDs with p values derived from pairwise Student's t tests, except where otherwise noted. ELDA (http://bioinf.wehi.edu.au/software/elda) was used to estimate stem cell frequencies.

SUPPLEMENTAL INFORMATION

Supplemental Information includes Supplemental Experimental Procedures, four figures, and four movies and can be found with this article online at http://dx.doi.org/10.1016/j.stemcr.2014.02.010.

ACKNOWLEDGMENTS

We thank Y. Zheng, L. Mack, J. Fitzpatrick, and J. Nguyen for technical assistance and equipment, J. Green and L. Bilezijkian for careful reading of the manuscript and helpful comments, and S. Ganley and D. Doan for administrative assistance. This work was supported by the Clayton Medical Research Foundation, The Breast Cancer Research Foundation, DoD Award number W81XWH-10-1-0891, Cancer Center Core grant P30 CA014195, and the Leona M. and Harry B. Helmsley Charitable Trust (#2012PG-MED002). This manuscript is dedicated to Wylie Vale in remembrance of his wisdom, humor, and irrepressible enthusiasm for science.

Received: August 21, 2013
Revised: February 22, 2014
Accepted: February 24, 2014
Published: April 3, 2014

REFERENCES

Adewumi, O., Aflatoonian, B., Ahrlund-Richter, L., Amit, M., Andrews, P.W., Beighton, G., Bello, P.A., Benvenisty, N., Berry, L.S., Bevan, S., et al.; International Stem Cell Initiative (2007). Characterization of human embryonic stem cell lines by the International Stem Cell Initiative. Nat. Biotechnol. *25*, 803–816.

Andersson, O., Korach-Andre, M., Reissmann, E., Ibáñez, C.F., and Bertolino, P. (2008). Growth/differentiation factor 3 signals through ALK7 and regulates accumulation of adipose tissue and diet-induced obesity. Proc. Natl. Acad. Sci. USA *105*, 7252–7256.

Ben-Porath, I., Thomson, M.W., Carey, V.J., Ge, R., Bell, G.W., Regev, A., and Weinberg, R.A. (2008). An embryonic stem cell-like gene expression signature in poorly differentiated aggressive human tumors. Nat. Genet. *40*, 499–507.

Bianco, C., Adkins, H.B., Wechselberger, C., Seno, M., Normanno, N., De Luca, A., Sun, Y., Khan, N., Kenney, N., Ebert, A., et al. (2002). Cripto-1 activates nodal- and ALK4-dependent and -independent signaling pathways in mammary epithelial Cells. Mol. Cell. Biol. *22*, 2586–2597.

Bianco, C., Strizzi, L., Mancino, M., Watanabe, K., Gonzales, M., Hamada, S., Raafat, A., Sahlah, L., Chang, C., Sotgia, F., et al. (2008). Regulation of Cripto-1 signaling and biological activity by caveolin-1 in mammary epithelial cells. Am. J. Pathol. *172*, 345–357.

Bianco, C., Rangel, M.C., Castro, N.P., Nagaoka, T., Rollman, K., Gonzales, M., and Salomon, D.S. (2010). Role of Cripto-1 in stem cell maintenance and malignant progression. Am. J. Pathol. *177*, 532–540.

Debnath, J., Muthuswamy, S.K., and Brugge, J.S. (2003). Morphogenesis and oncogenesis of MCF-10A mammary epithelial acini grown in three-dimensional basement membrane cultures. Methods *30*, 256–268.

Dong, D., Ni, M., Li, J., Xiong, S., Ye, W., Virrey, J.J., Mao, C., Ye, R., Wang, M., Pen, L., et al. (2008). Critical role of the stress chaperone GRP78/BiP in tumor proliferation, survival, and tumor angiogenesis in transgene-induced mammary tumor development. Cancer Res. *68*, 498–505.

Dontu, G., Abdallah, W.M., Foley, J.M., Jackson, K.W., Clarke, M.F., Kawamura, M.J., and Wicha, M.S. (2003). In vitro propagation and transcriptional profiling of human mammary stem/progenitor cells. Genes Dev. *17*, 1253–1270.

Ehninger, A., and Trumpp, A. (2011). The bone marrow stem cell niche grows up: mesenchymal stem cells and macrophages move in. J. Exp. Med. *208*, 421–428.

Gong, Y.P., Yarrow, P.M., Carmalt, H.L., Kwun, S.Y., Kennedy, C.W., Lin, B.P., Xing, P.X., and Gillett, D.J. (2007). Overexpression of Cripto and its prognostic significance in breast cancer: a study with long-term survival. Eur. J. Surg. Oncol. *33*, 438–443.

Gray, P.C., and Vale, W. (2012). Cripto/GRP78 modulation of the TGF-β pathway in development and oncogenesis. FEBS Lett. *586*, 1836–1845.

Gray, P.C., Harrison, C.A., and Vale, W. (2003). Cripto forms a complex with activin and type II activin receptors and can block activin signaling. Proc. Natl. Acad. Sci. USA *100*, 5193–5198.

Gyorki, D.E., Asselin-Labat, M.L., van Rooijen, N., Lindeman, G.J., and Visvader, J.E. (2009). Resident macrophages influence stem cell activity in the mammary gland. Breast Cancer Res. *11*, R62.

Heijmans, J., van Lidth de Jeude, J.F., Koo, B.K., Rosekrans, S.L., Wielenga, M.C., van de Wetering, M., Ferrante, M., Lee, A.S., Onderwater, J.J., Paton, J.C., et al. (2013). ER stress causes rapid loss of intestinal epithelial stemness through activation of the unfolded protein response. Cell Rep. *3*, 1128–1139.

Hough, S.R., Laslett, A.L., Grimmond, S.B., Kolle, G., and Pera, M.F. (2009). A continuum of cell states spans pluripotency and lineage commitment in human embryonic stem cells. PLoS ONE *4*, e7708.

Jones, D.L., and Wagers, A.J. (2008). No place like home: anatomy and function of the stem cell niche. Nat. Rev. Mol. Cell Biol. *9*, 11–21.

Kelber, J.A., Shani, G., Booker, E.C., Vale, W.W., and Gray, P.C. (2008). Cripto is a noncompetitive activin antagonist that forms analogous signaling complexes with activin and nodal. J. Biol. Chem. *283*, 4490–4500.

Kelber, J.A., Panopoulos, A.D., Shani, G., Booker, E.C., Belmonte, J.C., Vale, W.W., and Gray, P.C. (2009). Blockade of Cripto binding to cell surface GRP78 inhibits oncogenic Cripto signaling via MAPK/PI3K and Smad2/3 pathways. Oncogene *28*, 2324–2336.

Kenney, N.J., Huang, R.P., Johnson, G.R., Wu, J.X., Okamura, D., Matheny, W., Kordon, E., Gullick, W.J., Plowman, G., Smith, G.H., et al. (1995). Detection and location of amphiregulin and Cripto-1 expression in the developing postnatal mouse mammary gland. Mol. Reprod. Dev. *41*, 277–286.

Kenney, N.J., Smith, G.H., Lawrence, E., Barrett, J.C., and Salomon, D.S. (2001). Identification of Stem Cell Units in the Terminal End Bud and Duct of the Mouse Mammary Gland. J. Biomed. Biotechnol. *1*, 133–143.

Lee, A.S. (2007). GRP78 induction in cancer: therapeutic and prognostic implications. Cancer Res. *67*, 3496–3499.

Luo, S., Mao, C., Lee, B., and Lee, A.S. (2006). GRP78/BiP is required for cell proliferation and protecting the inner cell mass from apoptosis during early mouse embryonic development. Mol. Cell. Biol. *26*, 5688–5697.

Makarem, M., Kannan, N., Nguyen, L.V., Knapp, D.J., Balani, S., Prater, M.D., Stingl, J., Raouf, A., Nemirovsky, O., Eirew, P., and Eaves, C.J. (2013). Developmental changes in the in vitro activated regenerative activity of primitive mammary epithelial cells. PLoS Biol. *11*, e1001630.

Miharada, K., Karlsson, G., Rehn, M., Rörby, E., Siva, K., Cammenga, J., and Karlsson, S. (2011). Cripto regulates hematopoietic stem cells as a hypoxic-niche-related factor through cell surface receptor GRP78. Cell Stem Cell *9*, 330–344.

Mikaelian, I., Hovick, M., Silva, K.A., Burzenski, L.M., Shultz, L.D., Ackert-Bicknell, C.L., Cox, G.A., and Sundberg, J.P. (2006). Expression of terminal differentiation proteins defines stages of mouse mammary gland development. Vet. Pathol. *43*, 36–49.

Mizuno, H., Spike, B.T., Wahl, G.M., and Levine, A.J. (2010). Inactivation of p53 in breast cancers correlates with stem cell transcriptional signatures. Proc. Natl. Acad. Sci. USA *107*, 22745–22750.

Morkel, M., Huelsken, J., Wakamiya, M., Ding, J., van de Wetering, M., Clevers, H., Taketo, M.M., Behringer, R.R., Shen, M.M., and Birchmeier, W. (2003). Beta-catenin regulates Cripto- and Wnt3-dependent gene expression programs in mouse axis and mesoderm formation. Development *130*, 6283–6294.

Rangel, M.C., Karasawa, H., Castro, N.P., Nagaoka, T., Salomon, D.S., and Bianco, C. (2012). Role of Cripto-1 during epithelial-to-mesenchymal transition in development and cancer. Am. J. Pathol. *180*, 2188–2200.

Shackleton, M., Vaillant, F., Simpson, K.J., Stingl, J., Smyth, G.K., Asselin-Labat, M.L., Wu, L., Lindeman, G.J., and Visvader, J.E. (2006). Generation of a functional mammary gland from a single stem cell. Nature *439*, 84–88.

Shani, G., Fischer, W.H., Justice, N.J., Kelber, J.A., Vale, W., and Gray, P.C. (2008). GRP78 and Cripto form a complex at the cell surface and collaborate to inhibit transforming growth factor beta signaling and enhance cell growth. Mol. Cell. Biol. *28*, 666–677.

Spike, B.T., and Wahl, G.M. (2011). p53, Stem Cells, and Reprogramming: Tumor Suppression beyond Guarding the Genome. Genes Cancer *2*, 404–419.

Spike, B.T., Engle, D.D., Lin, J.C., Cheung, S.K., La, J., and Wahl, G.M. (2012). A mammary stem cell population identified and characterized in late embryogenesis reveals similarities to human breast cancer. Cell Stem Cell *10*, 183–197.

Spradling, A., Drummond-Barbosa, D., and Kai, T. (2001). Stem cells find their niche. Nature *414*, 98–104.

Stingl, J., Eirew, P., Ricketson, I., Shackleton, M., Vaillant, F., Choi, D., Li, H.I., and Eaves, C.J. (2006). Purification and unique properties of mammary epithelial stem cells. Nature *439*, 993–997.

Vaillant, F., Lindeman, G.J., and Visvader, J.E. (2011). Jekyll or Hyde: does Matrigel provide a more or less physiological environment in mammary repopulating assays? Breast Cancer Res. *13*, 108.

Van Keymeulen, A., Rocha, A.S., Ousset, M., Beck, B., Bouvencourt, G., Rock, J., Sharma, N., Dekoninck, S., and Blanpain, C. (2011). Distinct stem cells contribute to mammary gland development and maintenance. Nature *479*, 189–193.

Veltmaat, J.M., Mailleux, A.A., Thiery, J.P., and Bellusci, S. (2003). Mouse embryonic mammogenesis as a model for the molecular regulation of pattern formation. Differentiation *71*, 1–17.

Wey, S., Luo, B., and Lee, A.S. (2012a). Acute inducible ablation of GRP78 reveals its role in hematopoietic stem cell survival, lymphogenesis and regulation of stress signaling. PLoS ONE *7*, e39047.

Wey, S., Luo, B., Tseng, C.C., Ni, M., Zhou, H., Fu, Y., Bhojwani, D., Carroll, W.L., and Lee, A.S. (2012b). Inducible knockout of GRP78/BiP in the hematopoietic system suppresses Pten-null leukemogenesis and AKT oncogenic signaling. Blood *119*, 817–825.

Yeo, C., and Whitman, M. (2001). Nodal signals to Smads through Cripto-dependent and Cripto-independent mechanisms. Mol. Cell *7*, 949–957.

Zeng, Y.A., and Nusse, R. (2010). Wnt proteins are self-renewal factors for mammary stem cells and promote their long-term expansion in culture. Cell Stem Cell *6*, 568–577.

Zhang, Y., Liu, R., Ni, M., Gill, P., and Lee, A.S. (2010). Cell surface relocalization of the endoplasmic reticulum chaperone and unfolded protein response regulator GRP78/BiP. J. Biol. Chem. *285*, 15065–15075.

Stem Cell Reports, Volume *2*

Supplemental Information

CRIPTO/GRP78 Signaling Maintains Fetal and Adult Mammary Stem Cells Ex Vivo

Benjamin T. Spike, Jonathan A. Kelber, Evan Booker, Madhuri Kalathur, Rose Rodewald, Julia Lipianskaya, Justin La, Marielle He, Tracy Wright, Richard Klemke, Geoffrey M. Wahl, and Peter C. Gray

Inventory of Supplemental Information:

4 Supplemental Figures:

Figure S1 is related to Figure 1. It shows additional details on the structure, purification and quality control of ALK4^{L75A}-Fc, the Cripto antagonist used throughout the manuscript.

Figure S2 is also related to Figure 1.This figure shows additional validation of the effects of Cripto and ALK4^{L75A}-Fc on the cellular behavior of the human mammary epithelial cell line (MCF10A) in diverse contexts.

Figure S3 is related to Figure 3. It shows representative fetal mammary stem cell derived colonies under the influence of Cripto pathway agonism or antagonism and a demonstration of these influences in fibroblast co-cultures.

Figure S4 is related to Figure 4 and provides representative flow cytometric and tissue histologic validation of transplant data scored in the main figure, composites images of additional representative colonies derived from GRP78^{high} and GRP78^{low} adult mammary epithelial populations, boundaries used to distinguish them during cell sorting, and alternative graphical representations of their differential transplant and *in vitro* serial passage capacity.

4 Supplemental Movies:

These movies are representative time lapse video microscopy of MCF10A-V (control) and MCF10A-Cr (CRIPTO-overexpressing) cells and illustrate a CRIPTO-dependent increase in cell motility that is blocked by ALK4^{L75A}-Fc.

Movie S1. MCF10A-V; IgG-treated
Movie S2. MCF10A-Cr; IgG-treated
Movie S3. MCF10A-V; ALK4^{L75A}-Fc-treated
Movie S4. MCF10A-Cr; ALK4^{L75A}-Fc-treated

Supplemental methods:

These provide detail on time-lapse microscopy, expression and purification of ALK4^{L75A}-Fc and production of GRP78 antibodies.

Supplemental references:

These references are comprised of those that relate specifically to the Detailed Experimental Procedures and Supplemental Figures.

Supplemental Figures

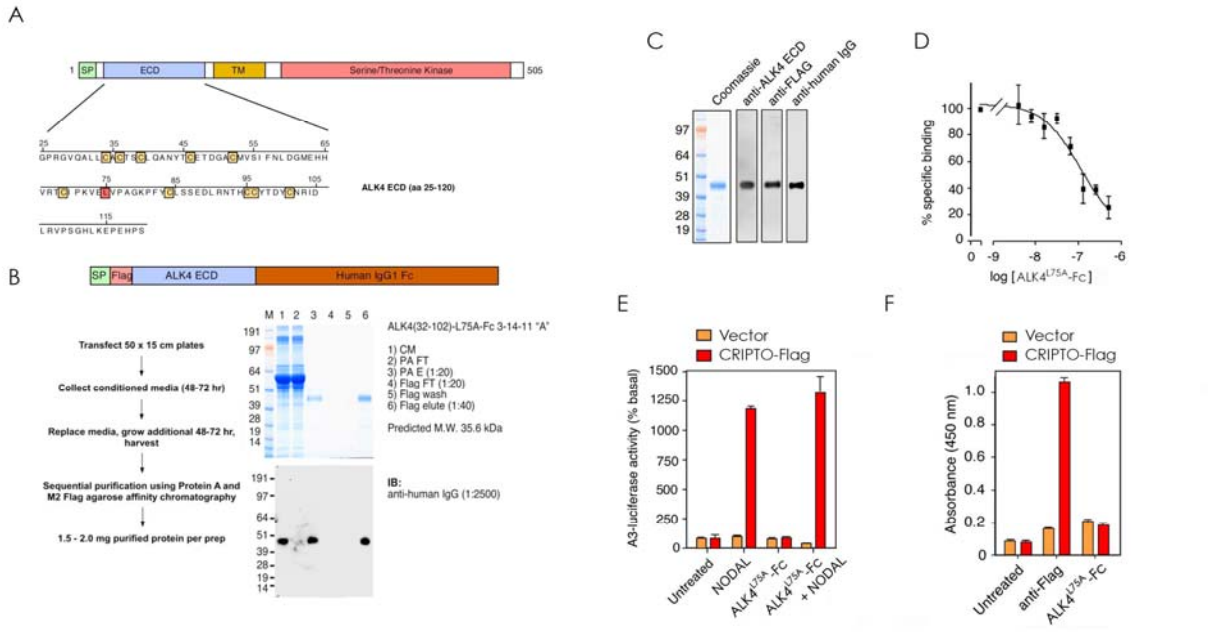

Figure S1, related to Figure 1. Structure, purification and validation of ALK4^{L75A}-Fc. (*A*) Human ALK4 consists of an N-terminal signal peptide, an extracellular domain (ECD), a transmembrane domain, and a cytoplasmic domain containing a serine/threonine protein kinase. ECD aa 25-120 are shown with conserved cysteine residues boxed and shaded yellow and the leucine at position 75 boxed and shaded red. The L75A mutation blocks ALK4/ACTIVIN binding without affecting ALK4/CRIPTO binding and was incoporated for increased CRIPTO specificity. (*B*) Diagram of the ALK4^{L75A}-Fc construct (top). ALK4^{L75A}-Fc was purified by sequential Flag agarose and Protein A agarose chromatography (bottom). The predicted molecular mass of ALK4^{L75A}–Fc proteins is ~39 kDa while the apparent size as visualized by SDS-PAGE is ~45 kDa, likely due to glycosylation of the ALK4-ECD. (*C*) Confirmation of the purity and identity of recombinant ALK4^{L75A} -Fc by Coomassie staining and western blotting using the indicated antibodies. (*D*) Binding of ^{125}I-CRIPTO to intact 293T cells overexpressing wild type ALK4 in the presence of the indicated doses of ALK4^{L75A} –Fc. (*E*) 293T cells were transfected with CRIPTO-Flag vector or control vector together with a SMAD2-responsive reporter construct (A3-luciferase). Cells were treated as indicated and resulting luciferase activities were measured. (*F*) 293T cells were transfected with CRIPTO-Flag or control vector and cell surface-anchored CRIPTO-Flag protein was detected by treating intact cells with Flag antibody followed by anti-mouse-HRP secondary antibody or with ALK4^{L75A} –Fc followed by anti-human Fc-HRP secondary followed by intact cell ELISA. Two independent experiments were carried out using technical triplicates (D-F).

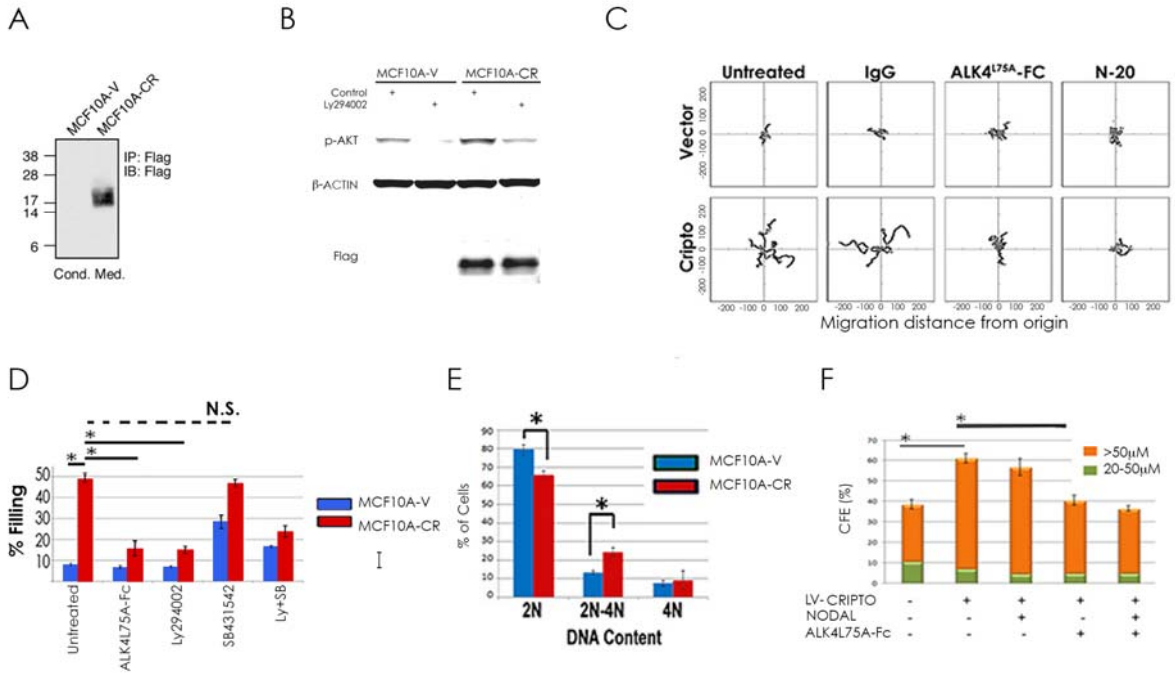

Figure S2, related to Figure 1. Effects of CRIPTO signaling and antagonism by ALK4^{L75A}-Fc in MCF10A Cells. (A) MCF10A-CR cells secrete CRIPTO-Flag. Conditioned media from MCF10A-V and MCF10A-CR cells was subjected to immunoprecipitation and western blotting with Flag antibody. (B) MCF10A-CR cells have higher phospho-AKT levels than MCF10A-V cells. Cell lysates were subjected to western blotting using antibodies directed toward phospho-AKT (p-AKT), actin or Flag as indicated. (C) Representative traces of migratory paths for MCF10A-CR and MCF10A-Vector control cells. MCF10A-CR cells exhibit elevated migration, a phenotype that is reversed by ALK4^{L75A}-Fc or the GRP78 neutralizing antibody N-20. See also Supplemental Movies S1-S4. (D) Suspension growth of MCF10A-V and MCF10A-CR cells was quantified by measuring the area filled by cells in images of individual wells. Cells were treated as indicated and data were normalized to areas measured for untreated MCF10A-V cells. *p<0.01 Student's t-tests. (E) Suspension cultured MCF10A-CR cells have a significantly greater portion of cells with >2N DNA content indicative of greater S-phase fraction and mitotic index. (F) ALK4^{L75A}-Fc inhibited acinar growth of MCF10A-CR cells in Matrigel cultures while NODAL treatment did not affect the number of acini (>50μm) observed in the presence or absence of ALK4^{L75A}-Fc. *p<0.05 t-tests. Results of two independent experiments with two replicates each are shown (D-F).

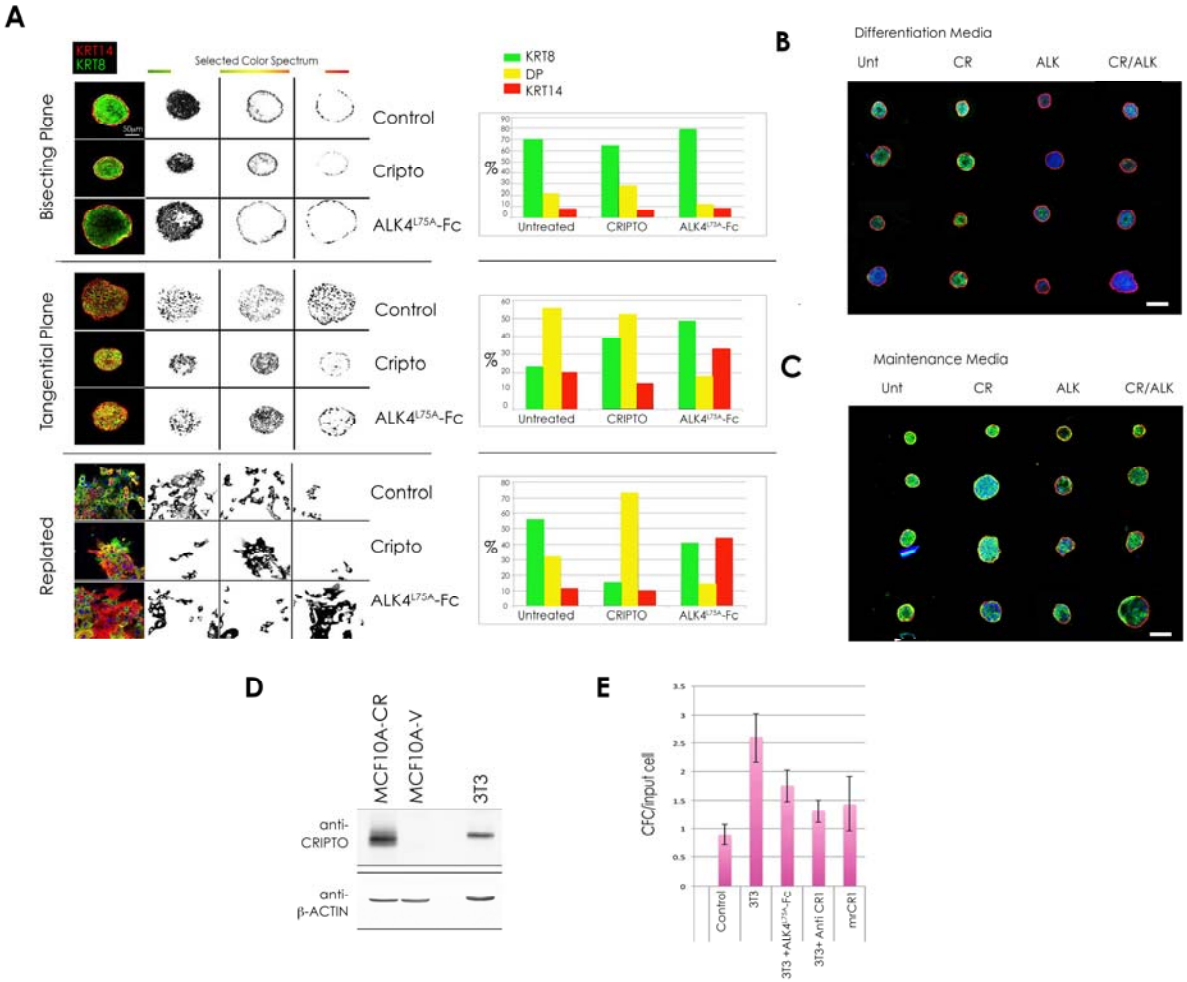

Figure S3, relates to Figure 3. Effects of CRIPTO stimulation or blockade on fMaSC derived organoids. (A) Representative organoids stained for Keratin 8 (green) and Keratin 14 (red) were quantified for distinct and overlapping keratin area (upper two panel sets) or the number of cells bearing distinct keratin expression patterns (bottom panels). Total pixels at the green, red and intermediate color ranges were selected and tallied in Adobe Photoshop for a central cross section (top panels) or peripheral section (middle panels) of day 7 organoids. In addition, nuclei contained within cells with predominantly KRT14, KRT8 or mixed staining cells were tallied following adherence and spread of individual colonies (bottom panels). In each case, ALK4^{L75A}-Fc treated colonies had more keratin single positive content relative to double positive content. Scale Bar = 50μm. (B, C) Composite images of additional representative organoids stained for Keratin 8 and Keratin 14 following growth under CRIPTO treatment or ALK4^{L75A}-Fc treatment in differentiation media (*B*) or maintenance media (*C*). Scale Bars = 100 μm. (D) Anti-CRIPTO western blot of 3T3 fibroblast lysates in comparison with control MCF10A-V and MCF10A-CR cells. (E) Quantification of colony forming cell (CFC) numbers relative to epithelial input cell number following co-culture of fMaSC derived organoids with 3T3 fibroblasts. 3T3 co-culture leads to increased clonogenic growth upon subsequent plating in 2 dimensions and this effect is partially reversed by ALK4^{L75A}-Fc or anti-CRIPTO antibodies. Statistical test = pairwise Student's t-test. A representative experiment using technical duplicates is shown.

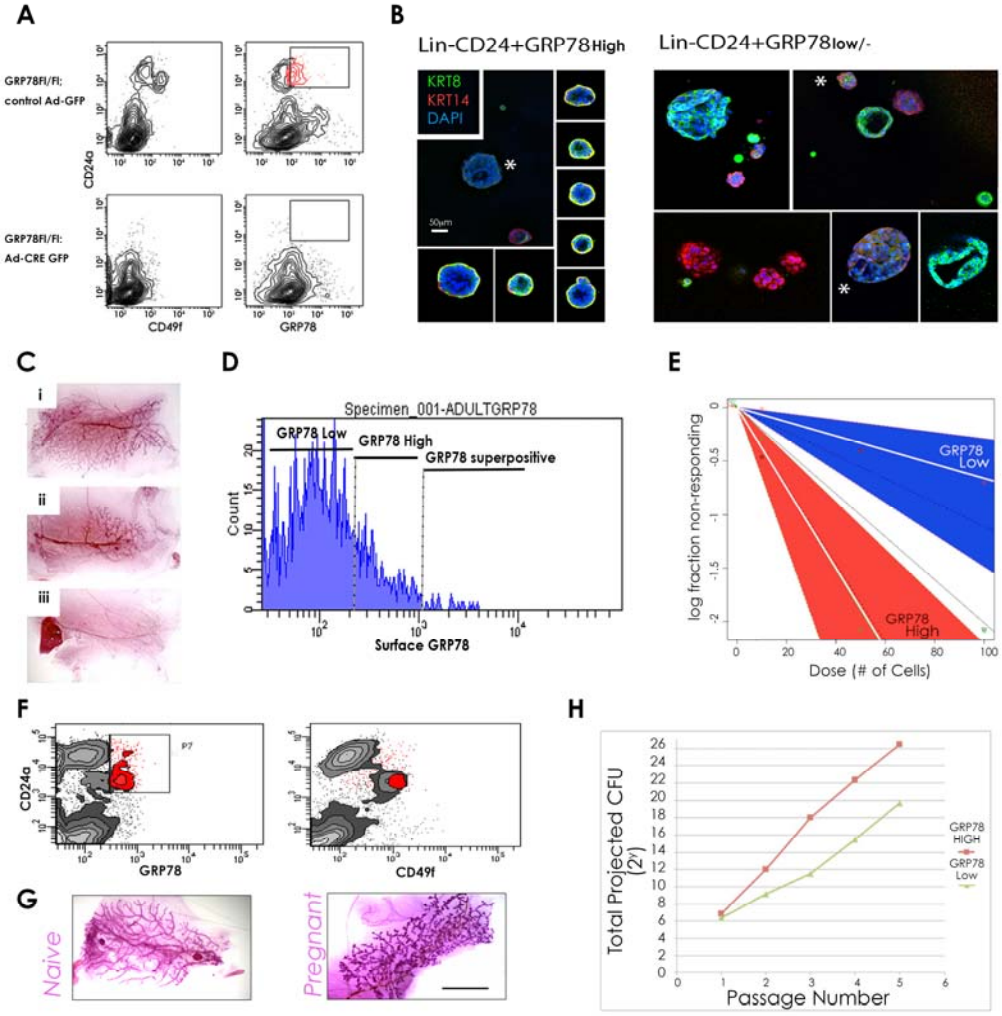

Figure S4, relating to Figure 4. Characterization of adult mammary epithelial cells with differing expression of cell surface GRP78. (A) Flow cytometric analysis of transplanted, conditionally GRP78-ablated mammary epithelial cells (GRP78Fl/Fl; Ad-CRE, lower panels) and control mammary epithelial cells (GRP78Fl/Fl; control Ad-GFP; upper panels) following 12 weeks outgrowth. (B) $GRP78^{high}$-derived colonies and $GRP78^{low}$-derived colonies collected from 2 independent experiments. KRT 8/14 co-labeling colonies were rare in the $GRP78^{low}$ population while, conversely, colonies lacking KRT 8/14 co-labeling were more rare in the $GRP78^{high}$ population than in the $GRP78^{low}$ population (*). Scale Bar = 50 μm, applies to all panels. (C, i-iii) Carmine stained whole mounts of transplanted mammary glands used to visualize the extent of fat pad filling by mammary ductal epithelia. Glands with 50-100% fatpad filling were scored as outgrowths. (D) Histogram representation of GRP78 positivity in the Lineage+ $CD24^{med}$ fraction of the normal mammary epithelium indicating approximate gating used to isolate $GRP78^{Low\text{-}Neg.}$, $GRP78^{high}$ and $GRP78^{high+}$ super-positive populations. (E) Limiting dilution analysis data for $GRP78^{low}$ cells (white line in blue region), $GRP78^{high}$ cells (white line in red region) and GRP78 super positive cells (black line; $GRP78^{high+}$). (F) Flow cytometric analysis of secondary transplants resulting from transplanted $GRP78^{high}$ cells. The lineage negative profiles are indistinguishable from normal endogenous mammary gland profiles and include luminal and myeoepithelial lineages and a $GRP78^{high}$ fraction. (G) Tertiary outgrowths from serially transplanted $GRP78^{high}$ cells. (H) Absolute cumulative colony forming units (CFU) calculated over serial passages in maintenance media (colonies produced/fraction of original cells plated at each round). Results of one experiment are shown. Subsequent experiments followed the same trend. Scale Bar = 1cm.

Supplemental Movies:

Supplemental Movie S1. MCF10A-V untreated

Supplemental Movie S2. MCF10A-V ALK4^{L75A}-Fc

Supplemental Movie S3. MCF10A-CR untreated

Supplemental Movie S4. MCF10A-CR ALK4^{L75A}-Fc

Supplemental Methods:

Expression and Purification of ALK4^{L75A}-Fc

ALK4^{L75A}-Fc was purified according to previously described methods (Harrison et al., 2004). 293T cells were plated in DMEM + 10% FBS + Ciproflaxin at 4x10^6 cells/15-cm plate coated with poly-D-lysine (up to 50+ plates). ~16 h following plating, cells were transfected with ALK4^{L75A}–Fc DNA in phenol red free DMEM containing 2.5% FBS using 24 μg DNA/36 μg PEI transfection reagent per plate. After transfection, cells were incubated ~48-72 hr at 37 degrees to allow protein expression and accumulation. Conditioned media was then collected, filtered through a 0.2 μm filter and neutralized by addition of 1/10th volume 1 M Tris pH 8. An additional 20 ml fresh phenol red free DMEM + 2.5% FBS was added to each plate and following an additional 48 hr conditioned media was again collected, filtered and neutralized.

ALK4^{L75A}–Fc proteins were purified by sequential protein A and M2-Flag agarose affinity chromatography. 10 cm x 1 cm columns were used with a large volume adaptor at the top for the protein A affinity column and ~3-5 ml affinity resin was used for each column. The protein A agarose bed was equilibrated with at least 10 column volumes protein A IgG binding buffer (21001 Pierce). Filtered, neutralized conditioned media was then gently added to column and allowed to flow through by gravity. The column was then washed extensively with protein A IgG binding buffer (> 10 column volumes) and the protein concentration of the last wash fraction was checked to make sure all unbound protein had been removed from the column. 10 mL elution buffer (0.1 M glycine, pH 2.8) was added to the column and collected into a tube containing 1 ml 1M Tris pH 8.8 to neutralize the eluate. Following elution, the protein A column was washed with an additional 2 column volumes of elution buffer and then the column was re-equilibrated with at least 10 column volumes of protein A IgG binding buffer. The M2-Flag column was equilibrated by washing with 10 column volumes of PBS. The sample to be purified (Protein A eluate) was loaded onto the Flag agarose column and allowed to flow through by

gravity. The flow through material was then loaded onto the column once more and allowed to flow through. The Flag agarose column was washed with 10 column volumes of Flag Wash Buffer (TBS) and then eluted with 10 ml of elution buffer (0.1 M Glycine pH 2.8) into a tube containing 1 ml Tris HCl pH 8.0. Samples were concentrated and buffer exchanged with PBS using an Amicon Ultra centricel with a 30 kDa cutoff (Millipore). Samples were centrifuged 3 times at 2750 rpm for 20 min at 4 degrees C using a Beckman J-6M swinging bucket centrifuge with adaptors for 50 ml tubes. Concentrated samples were typically between 1-5 mg/ml and 2-5 mg of pure protein was generally obtained for each set of 50 plates. After use, columns were stored in binding buffer containing 0.05% azide at 4 degrees.

^{125}I-CRIPTO binding

Recombinant mouse CRIPTO (R&D Systems) was iodinated and used for intact cell binding assays as previously described (Kelber et al., 2009).

Production of GRP78 antibody

Antisera were raised against synthetic amino acids 19-39 of human GRP78 or amino acids 81-97 of mouse CRIPTO conjugated to human α-globulins via bisdiazotized benzidine using a protocol previously described in detail for inhibin subunits (Vaughan et al., 1989). Antisera were produced in rabbit using complete Freund's adjuvant (initial injection) or incomplete Freund's adjuvant (booster injections) mixed with an equal volume of phosphate buffered saline containing hGRP(19-39)- or mCR(81-97) α-globulins conjugate. Host animals were immunized every 3 wk with 0.5 mg conjugate (initial injection) or 0.25 mg conjugate (booster injection) delivered in multiple intradermal sites. Rabbits were bled and sera were harvested 7 days after each booster injection. Rabbit #PBL 6197 (GRP78) and #PBL 6900 (CRIPTO) serum was used for these studies.

Time-Lapse Imaging and Migration Analysis

MCF10A-V or MCF10A-CR cells were plated on Matrigel (1:10 dilution) at $1x10^4$ cells/well in duplicate in a 24-well plate and allowed to adhere in the presence of the following treatments (untreated, 2 μg/mL Goat IgG, 10 μg/mL $ALK4^{L75A}$-Fc, or 2 μg/mL N-20) for four hours prior to imaging. Sequential images were captured at 10x magnification and 10-minute intervals for three different fields per well at 37 °C for ~14 hours. Cell migration dynamics were quantified for individual cells using Metamorph Imaging/Tracking software. Velocity (pixels/minute) and persistence (D-displacement/T-track length) values were calculated and averages were plotted and statistics were calculated using a 2-way ANOVA test and Graph Pad Prims. Representative rose plots were generated using cell position data from approximately 10 cells per condition relative to an x,y origin of 0,0 in Excel. Image stacks were exported from Metamorph and compiled into quick time movies.

Proliferation

Cells were plated in triplicate in 96 well plates and quantified at the indicated times on a Celigo microplate cytometer (Cyntellect).

Cell Cycle Analysis

Cells were incubated for 15 min at room temperature with 4 μg/ml Hoechst33342 DNA dye and with 1 μg/ml propidium iodide (PI). Hoechst+PI- cells were registered on an LSRII flow cytometer (BD) in linear scale with the major population designated as 2N DNA content.

Primary Cell Preparation

Cells were prepared according to the Stem Cell Technologies protocol with modifications

described previously that shorten the dissociation time (90 min) and omit trypsinization for fetal derived material (Spike et al., 2012).

Primary Cell Flow Cytometry

Flow cytometry and cell sorting were carried out as described previously (Spike et al., 2012) incorporating the polyclonal rabbit antibodies targeting GRP78 described above.

In Vitro Colony Formation Assays

For suspension cultures of MCF10A cells, 2-3 replicates of equivalent cell numbers were seeded at a density of 2000-5000 cells/ml in complete CnT-27 media and grown for up to 2 weeks in low adherence tissue culture plates with feeding every 5 days by media addition. Individual wells were photographed and the percentage of the field occupied by cells was quantified. Alternatively, cells were suspended in MCF10A media containing 1% methylcellulose and followed for 4 weeks and spheres were quantified and measured under phase contrast microscopy. For Matrigel cultures, cells were seeded at 5000 cells/ml and grown in 2% growth factor reduced Matrigel (BD Biosciences) in MCF10A media in 96 well low adherence dishes (Corning). For primary mouse mammary epithelia, cells were seeded in 2% Matrigel at the single cell densities described above or were seeded at the time of sorting as single cells per well in 96 well plates. Cells were isolated for serial passage with cell recovery solution (BD Biosciences) and trypsinization according to the manufacturer's recommendations. For confocal microscopy, cells were grown in 75% Matrigel on 8 well glass chamber slides. AKT activation was determined after four days of organoid culture followed by three hours of serum starvation with the indicated treatments. 3T3 co-culture experiments were carried out as previously described (Makarem et al., 2013), with minor modifications. Briefly, 3T3 fibroblasts were arrested with Mitomycin-C (10 μg/ml) and admixed with fMaSC cells. Cells were subsequently co-cultured in differentiation media with 2% Matrigel for 7 days before being plated at low

density into 2-dimensional culture with maintenance media and grown for 4 days for colony counting. Polyclonal rabbit antibodies directed against amino acids 81-97 of mouse CRIPTO were added to sequester CRIPTO where indicated.

RT-PCR

Relative mRNA expression levels of *TDGF1* (*CRIPTO*) were obtained using the comparative CT method between *TDGF1* directed Taqman assays (Mm03024051_g1, Applied Biosciences) and *HPRT* (Mm01324427_m1, Applied Biosciences). Samples were amplified as technical triplicates and quantified on an ABI 7900HT Fast Real-Time PCR system.

Immunostaining

Cells were fixed with 10% neutral buffered formalin (NBF) and CRIPTO or GRP78 protein was detected with the standard avidin-biotin immunoperoxidase procedures, sodium citrate antigen retrieval methods, and the VECTASTAIN Elite ABC Kit (Vector Laboratories) using rabbit polyclonal anti-CRIPTO (AbCam) 1:1000; goat polyclonal anti-GRP78 (SC Biotechnology) 1:400. Cytokeratin staining was conducted as previously described (Spike et al., 2012) using antibodies against KRT14 (AF-64, Covance, 1:1000), KRT8 (Troma-1, DSHB, 1:100) and DAPI 500 ng/ml. Whole mount immunofluorescent staining was carried out on adult sections as above for IHC and on E18.5 fetal mammary rudiments in suspension using goat antibody N-20 (1:400) to detect GRP78, KRT8 antibodies and DAPI as described above and polyclonal rabbit antibodies directed against amino acids 81-97 of mouse CRIPTO. Macrophages were detected with APC-conjugated anti-F4/80 antibodies (BM8, eBioscience, 1:250). The rudiments were fixed for 1hr in 10% neutral buffered formalin at 4°C, blocked and stained in 4% horse serum in PBS/0.1% Triton X-100 with primary antibodies and subsequently with species specific Alexa Fluor 488, 568 and/or 660 conjugated secondary antibodies, before mounting in Prolong Gold (Life Technologies) and imaging on a Zeiss LSM780 Microscope. The 2-dimensional cultures of

fMaSCs used for Ki67 detection (B56, BD, 1:100) were treated as indicated on day 1 and day 6 and were then fixed on day 7 with 10% NBF and cold Methanol Acetone (3:1) prior to staining.

Mammary Fat Pad Transplantation and Analysis

Mammary transplantation analyses were conducted as previously described (Spike et al., 2012), using ELDA to estimate stem cell frequencies (http://bioinf.wehi.edu.au/software/elda/). Here, donor material comprised primary cells grown in 2% Matrigel as described above for 5 days under the indicated treatments. 20 colonies (by dilution) were injected with Matrigel into cleared fat pads of 21 day old SCID hosts (Charles River) and outgrowth was determined at 8-12 weeks by carmine staining as previously described (Figure S4Ci-Ciii) (Spike et al., 2012). Alternatively, donor material comprised primary adult mammary epithelial cells from wild type mice sorted as described previously (Stingl et al., 2006) or sorted on the basis of surface GRP78 expression detected with polyclonal GRP78 antibodies. Additionally, cells from GRP78 floxed mice (a kind gift of Amy Lee, University of Southern California) were sorted as above and transduced by 60 min spinoculation with Adeno-viral vectors expressing GFP and CRE recombinase or GFP alone, grown overnight in maintenance media, sorted for GFP expression and transplanted as described.

Supplemental References:

Harrison CA, Gray PC, Fischer WH, Donaldson C, Choe S, et al. (2004) An activin mutant with disrupted ALK4 binding blocks signaling via type II receptors. J Biol Chem 279: 28036-28044.

Kelber, J.A., Shani, G., Booker, E.C., Vale, W.W., and Gray, P.C. (2008). Cripto is a noncompetitive activin antagonist that forms analogous signaling complexes with activin and nodal. J Biol Chem *283*, 4490-4500.

Kelber, J.A., Panopoulos, A.D., Shani, G., Booker, E.C., Belmonte, J.C., Vale, W.W., and Gray, P.C. (2009). Blockade of Cripto binding to cell surface GRP78 inhibits oncogenic Cripto signaling via MAPK/PI3K and Smad2/3 pathways. Oncogene *28*, 2324-2336.

Makarem, M., Kannan, N., Nguyen, L.V., Knapp, D.J., Balani, S., Prater, M.D., Stingl, J., Raouf, A., Nemirovsky, O., Eirew, P.*, et al.* (2013). Developmental changes in the in vitro activated regenerative activity of primitive mammary epithelial cells. PLoS Biol *11*, e1001630.

Spike, B.T., Engle, D.D., Lin, J.C., Cheung, S.K., La, J., and Wahl, G.M. (2012). A mammary stem cell population identified and characterized in late embryogenesis reveals similarities to human breast cancer. Cell Stem Cell *10*, 183-197

Stingl, J., Eirew, P., Ricketson, I., Shackleton, M., Vaillant, F., Choi, D., Li, H.I., and Eaves, C.J. (2006). Purification and unique properties of mammary epithelial stem cells. Nature *439*, 993-997.

Vaughan JM, Rivier J, Corrigan AZ, McClintock R, Campen CA, et al. (1989) Detection and purification of inhibin using antisera generated against synthetic peptide fragments. In: Conn PM, editor. Methods in Enzymology. Orlando, FL: Academic Press, Inc. pp. 588-617.